

DOCUMENTATION PAGE

Form Approved
OMB No. 0704-0188

AD-A265 406



Information is estimated to average 1 hour per response, including the time for reviewing instructions, searching existing data sources, gathering and reviewing the collection of information, sending comments regarding this burden estimate or any other aspect of this collection of information, including suggestions for reducing this burden, to Washington Headquarters Services, Directorate for Information Operations and Reports, 1215 Jefferson Avenue, Washington, DC 20540, and to the Office of Management and Budget, Paperwork Reduction Project (0704-0188), Washington, DC 20503.

2. REPORT DATE
Fall 1992

3. REPORT TYPE AND DATES COVERED
THESIS

4. TITLE AND SUBTITLE
Thermodynamic Structure of Subsidence Inversions in the Atlantic Subtropical Anticyclone Regime

5. FUNDING NUMBERS



6. AUTHOR(S)
Captain Mark B. Miller

7. PERFORMING ORGANIZATION NAME(S) AND ADDRESS(ES)
AFIT Student Attending: Florida State University

8. PERFORMING ORGANIZATION REPORT NUMBER
AFIT/CI/CIA-92-116

9. SPONSORING/MONITORING AGENCY NAME(S) AND ADDRESS(ES)
AFIT/CI
Wright-Patterson AFB OH 45433-6583

10. SPONSORING/MONITORING AGENCY REPORT NUMBER

11. SUPPLEMENTARY NOTES

12a. DISTRIBUTION AVAILABILITY STATEMENT
Approved for Public Release IAW 190-1
Distributed Unlimited
ERNEST A. HAYGOOD, Captain, USAF
Executive Officer

DTIC
ELECTE
JUN 07 1993
S A D

13. ABSTRACT (Maximum 200 words)

93 0 04 068

93-12642
Barcode

87P8

14. SUBJECT TERMS

15. NUMBER OF PAGES
85

16. PRICE CODE

17. SECURITY CLASSIFICATION OF REPORT

18. SECURITY CLASSIFICATION OF THIS PAGE

19. SECURITY CLASSIFICATION OF ABSTRACT

20. LIMITATION OF ABSTRACT

GENERAL INSTRUCTIONS FOR COMPLETING SF 298

The Report Documentation Page (RDP) is used in announcing and cataloging reports. It is important that this information be consistent with the rest of the report, particularly the cover and title page. Instructions for filling in each block of the form follow. It is important to *stay within the lines* to meet optical scanning requirements.

Block 1. Agency Use Only (Leave blank).

Block 2. Report Date. Full publication date including day, month, and year, if available (e.g. 1 Jan 88). Must cite at least the year.

Block 3. Type of Report and Dates Covered. State whether report is interim, final, etc. If applicable, enter inclusive report dates (e.g. 10 Jun 87 - 30 Jun 88).

Block 4. Title and Subtitle. A title is taken from the part of the report that provides the most meaningful and complete information. When a report is prepared in more than one volume, repeat the primary title, add volume number, and include subtitle for the specific volume. On classified documents enter the title classification in parentheses.

Block 5. Funding Numbers. To include contract and grant numbers; may include program element number(s), project number(s), task number(s), and work unit number(s). Use the following labels:

C - Contract	PR - Project
G - Grant	TA - Task
PE - Program Element	WU - Work Unit Accession No.

Block 6. Author(s). Name(s) of person(s) responsible for writing the report, performing the research, or credited with the content of the report. If editor or compiler, include the name(s).

Block 7. Performing Organization Name and Address(es). Self-explanatory.

Block 8. Performing Organization Report Number. Enter the unique alphanumeric report number(s) assigned by the organization performing the report.

Block 9. Sponsoring/Monitoring Agency Name(s) and Address(es). Self-explanatory.

Block 10. Sponsoring/Monitoring Agency Report Number. (If known)

Block 11. Supplementary Notes. Enter information not included elsewhere such as: Prepared in cooperation with..., Trans. of..., To be published in..., When a report is revised, include a statement whether the new report supersedes or supplements the older report.

Block 12a. Distribution/Availability Statement. Denotes public availability or limitations. Cite any availability to the public. Enter additional limitations or special markings in all capitals (e.g. NOFORN, REL, ITAR).

DOD - See DoDD 5230.24, "Distribution Statements on Technical Documents."

DOE - See authorities.

NASA - See Handbook NHB 2200.2.

NTIS - Leave blank.

Block 12b. Distribution Code.

DOD - Leave blank.

DOE - Enter DOE distribution categories from the Standard Distribution for Unclassified Scientific and Technical Reports.

NASA - Leave blank.

NTIS - Leave blank.

Block 13. Abstract. Include a brief (Maximum 200 words) factual summary of the most significant information contained in the report.

Block 14. Subject Term. Keywords or phrases that define the subject of the report.

Block 15. Number of Pages. Enter the total number of pages.

Block 16. Price Code. Enter appropriate price code (NTIS only)

Blocks 17 - 19. Security Classifications. Self-explanatory. Enter U.S. Security Classification in accordance with U.S. Security Regulations (i.e., UNCLASSIFIED). If form contains classified information, stamp classification on the top and bottom of the page.

Block 20. Limitation of Abstract. This block must be completed to assign a limitation to the abstract. Enter either UL (unlimited) or SAR (same as report). An entry in this block is necessary if the abstract is to be limited. If blank, the abstract is assumed to be unlimited.

THE FLORIDA STATE UNIVERSITY
COLLEGE OF ARTS AND SCIENCES

THERMODYNAMIC STRUCTURE OF SUBSIDENCE
INVERSIONS IN THE ATLANTIC SUBTROPICAL
ANTICYCLONE REGIME

By

MARK B. MILLER

A Thesis submitted to the
Department of Meteorology
in partial fulfillment of the
requirements for the degree of
Master of Science

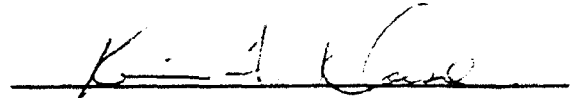
Degree Awarded:

Fall Semester, 1992

Accession For	
NTIS	✓
DTIC	
Other	
Justification	
By	
Distribution	
Availability	
Dist	Availability
A-1	Special

DTIC QUALITY INSPECTED 2

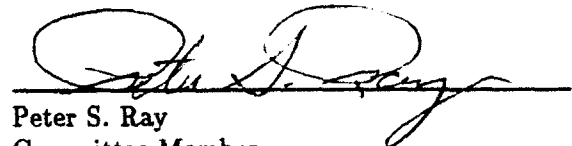
The members of the Committee approve the thesis of Mark B. Miller defended on
July 24, 1992.



Kevin A. Kloesel
Professor Directing Thesis



Paul H. Ruscher
Committee Member



Peter S. Ray
Committee Member

Dedication

This thesis is dedicated to my parents, Bob and Linda Miller, who did an excellent job of training their three sons in the way that they should go.

Acknowledgments

I would like to express my sincerest thanks and extreme gratitude to my major professor, Dr. Kevin A. Kloesel for his guidance and unending support in the development of this thesis. I would also like to thank my committee members, Dr. Paul H. Ruscher and Dr. Peter S. Ray, for their help and valuable input during the final stages of the completion of this work. I thank the United States Air Force for selecting me to attend school for my Master's Degree. I also thank Mr. Don Paugh for lending me his computer monitor at a time when my work on my home computer was crucial. I thank my wonderful wife, Susan, whose love and support pulled me through this most challenging time in my life. Proverbs 31:10 says, "A wife of noble character, who can find?" I found such a wife. Last, but not least, I thank my God who gave me the strength and perseverance to endure it all.

Contents

Dedication	iii
Acknowledgments	iv
List of Figures	vi
Abstract	ix
1 Introduction	1
2 Data Used	9
3 Subsidence Inversion Climatology	13
3.1 Evidence of the Subsidence Inversion	13
3.2 Thermodynamic Structure of the Subsidence Inversion	21
4 Above-Subsidence Inversion Structure	32
4.1 Climatology of Subsidence Inversions With Moist Nose Structure	34
4.2 Climatology of Subsidence Inversions Without Moist Nose Structure	44
4.3 Differences Between the Thermodynamic Structure of Subsidence Inversions With and Without Moist Noses	51
5 Source of Moisture Above the Subsidence Inversion	61
6 Conclusion	70
References	74
Vita	76

List of Figures

1	Temperature and dewpoint plot on a Skew-T Log P diagram, showing a typical profile of a subsidence inversion.	3
2	Vertical profile of total mixing ratio used in climate models (from Stull, 1988).	5
3	Profile of the complex moisture structure over the subsidence inversion in the eastern Pacific during FIRE (Klagesel, 1992).	6
4	Temperature and dewpoint profile on a Skew-T Log P diagram showing an example of a complex moisture structure above the subsidence inversion in the eastern Atlantic Ocean.	8
5	Map of ASTEX study area in the eastern Atlantic Ocean (FIRE Project Office and ASTEX Working Group, 1992).	10
6	Mean sea level pressure plot of the Atlantic Ocean depicting the mean position and intensity of the subtropical anticyclone for the month of June, 1980-1990.	14
7	Time series plot of surface pressure for June 1980. Fifty-three data points were available for this year.	15
8	Histogram of the difference of mixing ratio between the top and bottom of the inversion (in g/kg). Negative values indicate drying within the inversion. The number of inversions to the right of the '0' column have values of $\Delta q \geq 0$	17
9	Mean plot of temperature and mixing ratio at the surface, inversion base and inversion top for all soundings with subsidence inversions for Lajes in June 1980-1990.	18
10	Skew T Log P diagrams depicting temperature and dewpoint profiles of (a) a sounding containing a superadiabatic lapse rate, (b) an unreliable sounding, (c) a sounding in which moisture may have subsided into the inversion, and (d) a subsidence inversion in which the appearance of moisture increase within the inversion was due to the 30° C maximum dewpoint depression coding convention.	19
11	Mean temperature profile of boundary layer and subsidence inversion for all times (solid line), 00 UTC (long dash), and 12 UTC (short dash).	22
12	Mean mixing ratio profile of boundary layer and subsidence inversion for all times (solid line), 00 UTC (long dash), and 12 UTC (short dash).	23

13	Mean potential temperature profile of boundary layer and subsidence inversion for all times (solid line), 00 UTC (long dash), and 12 UTC (short dash).	24
14	Mean weekly temperature profile of the boundary layer and subsidence inversion. Each week is indicated as follows: Week 1, solid line; Week 2, long dash; Week 3, medium dash; Week 4, short dash.	27
15	Mean weekly mixing ratio profile of the boundary layer and subsidence inversion. Each week is indicated as follows: Week 1, solid line; Week 2, long dash; Week 3, medium dash; Week 4, short dash.	28
16	Mean weekly inversion strength (K/mb) for soundings with subsidence inversions.	30
17	Time series plot of temperature (T) and specific humidity (q) taken during ATEX on 26-29 September 1969 at 30°W/0°N (from Augstein et al., 1974).	33
18	Mean temperature profile of boundary layer and inversion for all subsidence inversions with a moist nose present for all times (solid line), 00 UTC (long dash), and 12 UTC (short dash).	35
19	Mean mixing ratio profile of boundary layer and inversion for all subsidence inversions with a moist nose present for all times (solid line), 00 UTC (long dash), and 12 UTC (short dash).	36
20	Weekly percentage of subsidence inversions with the moist nose present. . .	40
21	Mean weekly temperature profile of the boundary layer and inversion of subsidence inversions with moist noses. Each week is indicated as follows: Week 1, solid line; Week 2, long dash; Week 3, medium dash; Week 4, short dash. . .	41
22	Mean weekly mixing ratio profile of the boundary layer and inversion of subsidence inversions with moist noses. Each week is indicated as follows: Week 1, solid line; Week 2, long dash; Week 3, medium dash; Week 4, short dash.	42
23	Mean temperature profile of boundary layer and inversion for all subsidence inversions without a moist nose present for all times (solid line), 00 UTC (long dash), 12 UTC (short dash).	45
24	Mean mixing ratio profile of boundary layer and inversion for all subsidence inversions without a moist nose present for all times (solid line), 00 UTC (long dash), 12 UTC (short dash).	46
25	Mean weekly temperature profile of the boundary layer and subsidence inversion of subsidence inversions without moist noses. Each week is indicated as follows: Week 1, solid line; Week 2, long dash; Week 3, medium dash; Week 4, short dash.	49
26	Mean weekly mixing ratio profile of the boundary layer and subsidence inversion of subsidence inversions without moist noses. Each week is indicated as follows: Week 1, solid line; Week 2, long dash; Week 3, medium dash; Week 4, short dash.	50
27	Mean inversion strength of subsidence inversions with the moist nose (light stippled pattern) and without the moist nose present (grey pattern) for all times, 00 UTC and 12 UTC.	52
28	Mean weekly inversion strength of subsidence inversions with (light stippled pattern) and without the moist nose present (grey pattern).	54

29	Mean temperature and mixing ratio profiles of boundary layer and inversion for subsidence inversions with the moist nose (solid line and dot-short dash, respectively) and without the moist nose (long dash and dot-long dash, respectively).	55
30	Mean potential temperature profile for subsidence inversions with the moist noses (solid line) and without the moist noses (dashed line).	56
31	Mean weekly temperature profile for subsidence inversions with the moist nose (plots with hollow symbols) and without the moist nose (plots with filled symbols).	58
32	Mean weekly mixing ratio profile for subsidence inversions with the moist nose (plots with hollow symbols) and without the moist nose (plots with filled symbols).	59
33	Scatter diagram of mixing ratio (g/kg) above the subsidence inversion and subsidence inversion strength (K/mb).	63
34	Conserved variable diagram of the mean values of mixing ratio and equivalent potential temperature at the surface, inversion base and top and in the moist nose for all times, 00 UTC, 12 UTC, and Weeks 1 through 4 for all subsidence inversions with moist noses. The dashed line is a least-squares fit of the surface, inversion base and top values.	66
35	Mean global surface pressure pattern for the month of July (from Ahrens, 1991).	68

Abstract

Data obtained from the eastern Atlantic Ocean for June 1980-1990 were examined to determine the mean thermodynamic structure of the boundary layer, subsidence inversion layer, and free atmosphere above the subsidence inversion layer along the eastern periphery of the Atlantic subtropical anticyclone. Moist intrusions in the free atmosphere above the subsidence inversion were found to exist in many cases. Differences in the thermodynamic structure were found between soundings with and without the moist layer present above the subsidence inversion. The moist layer itself was discussed and possible sources for the moisture were examined.

Chapter 1

Introduction

Few studies have been accomplished to examine the characteristics of the cloud-topped *marine boundary layer* in the vicinity of the subtropical anticyclone over the Atlantic Ocean. Many experiments, such as ATEX (Atlantic Trade-Wind Experiment), BOMEX (Barbados Oceanographic and Meteorological Experiment), and GATE (GARP (Global Atmospheric Research Program) Atlantic Tropical Experiment), were conducted to examine the trade-wind regime in the northeastern Atlantic along the eastern periphery of the subtropical anticyclone (Augstein et al., 1973) or to collect data on convection in the tropics and its role in global atmospheric circulation (Nitta and Esbensen, 1974, Houze and Betts, 1981). Lilly (1968) examined the marine boundary layer off the coast of California in an effort to explain and predict features of the cloud layer over the ocean under strong subsidence inversions associated with the Pacific subtropical anticyclone. More recent studies along the eastern periphery of the Pacific subtropical anticyclone have also indicated that inversion and above inversion structure, as well as boundary layer cloud variations, are, in many

instances, controlled by synoptic scale processes associated with the subtropical anticyclone (Kloesel, 1992). The climatic importance of processes which affect oceanic cloud regimes was discussed by Randall et al. (1984), who stated that marine stratus and stratocumulus clouds play an important role in the earth's radiative energy budget due to their high albedo (20-40%) compared to that of the ocean (10%). A mere 4% increase in the area of the globe covered by low level stratus clouds would be sufficient to offset the 2-3 K predicted rise in global temperature due to doubling of carbon dioxide in the atmosphere (Randall et al., 1984).

To address the interaction between oceanic cloud regimes and climate, FIRE (First ISCCP (International Satellite Cloud Climatology Program) Regional Experiment)-Phase I was conducted. The goal of FIRE Phase I was to better understand boundary layer turbulence, cloud microphysics, and cloud radiation in nearly homogeneous stratocumulus cloud regimes in order to improve cloud and radiation parameterizations in climate models. ASTEX (Atlantic Stratocumulus Transition Experiment), conducted during June 1-28 1992, will provide data over a more broken stratocumulus regime (eastern Atlantic) to determine fractional cloudiness parameters and cloud break-up mechanisms. These data will also be used to validate and drive climate models (FIRE Project Office and ASTEX Working Group, 1992).

In preparation for ASTEX, this study was undertaken to better understand subsidence inversions in the eastern Atlantic around the eastern periphery of the subtropical anticyclone. Subsidence inversions over subtropical oceanic regions are inversions typically characterized by a distinct drying within the inversion layer (Figure 1). The free atmosphere

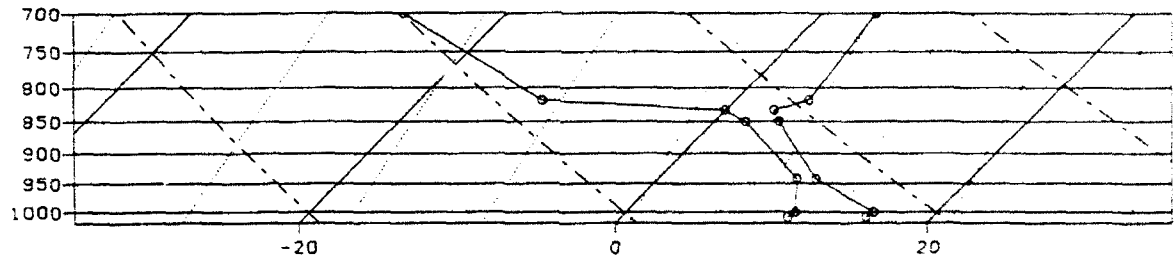


Figure 1: Temperature and dewpoint plot on a Skew-T Log P diagram, showing a typical profile of a subsidence inversion.

above the inversion is also characterized by subsidence associated with the semi-permanent anticyclone, which is present throughout the summer months. (HQ, Air Weather Service, 1961).

Historically, modelling of the upper boundary (inversion) of a cloud-topped marine boundary layer has been handled in a simplistic way (Figure 2). The free atmosphere above the subsidence inversion is typically considered to be uniformly dry, i.e. specific humidities are 1 g/kg or less. However, there may be a more complex moisture structure above the subsidence inversion which would complicate this simplistic initialization scheme (Kloesel, 1992). An example of this complex structure is shown in Figure 3. This profile, obtained during FIRE, shows a 30 mb thick layer of moist air above the subsidence inversion, with a region of dry air between the moist layer and the top of the inversion. The moist layer in Figure 3 and the moist layers described in this study do not contain cloud layers. The dewpoint depression in these layers is typically on the order of 9° C. However, although these layers are cloudless, it was previously shown with two boundary layer models that if they subside into the inversion layer, they can be entrained into the boundary layer with a resulting increase boundary layer cloud depth (Kloesel, 1992). Furthermore, lidar observations obtained during FIRE showed a sloping layer with high specific humidity values intersecting with the marine stratocumulus cloud layer, which had a cloud enhancing effect (Schiesow et al., 1990). Therefore, a better understanding of the existence of the moist layer is needed so that parameterizations of this feature can be incorporated into boundary layer models and, ultimately, climate models. This moist intrusion above the subsidence inversion, previously referred to as q -reversal (Kloesel and Albrecht, 1989), will be hereafter

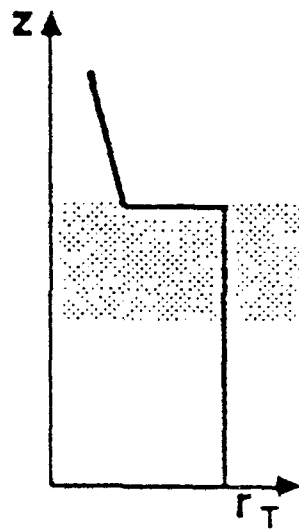


Figure 2: Vertical profile of total mixing ratio used in climate models (from Stull, 1988).

FIRE FLIGHT 3 SOUNDING 3

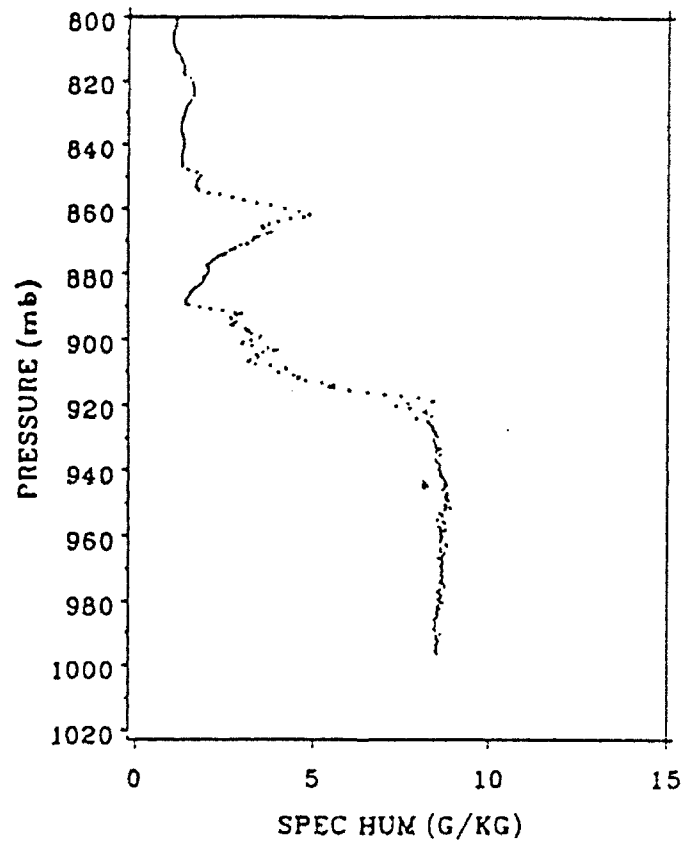


Figure 3: Profile of the complex moisture structure over the subsidence inversion in the eastern Pacific during FIRE (Kloesel, 1992).

referred to as a "moist nose" due to its appearance. The moist nose is defined as a maximum of mixing ratio that is 1 g/kg or more greater than the background mixing ratio profile. Figure 4 illustrates an atmosphere characterized by a multiple moist nose structure.

This thesis will present a climatology and examine characteristics of the subsidence inversion in the eastern Atlantic associated with the subtropical anticyclone to lay ground work for post-ASTEX research. Chapter 2 will explain the data used for this thesis. Chapter 3 will give the overall climatology of the subsidence inversion over the eastern Atlantic Ocean. Chapter 4 will discuss the thermodynamic structure above the subsidence inversion, and compare those subsidence inversions with the moist nose present to those subsidence inversions without a moist nose. Chapter 5 will theorize the possible causes of the moisture above the subsidence inversion with the use of a conserved variable diagram.

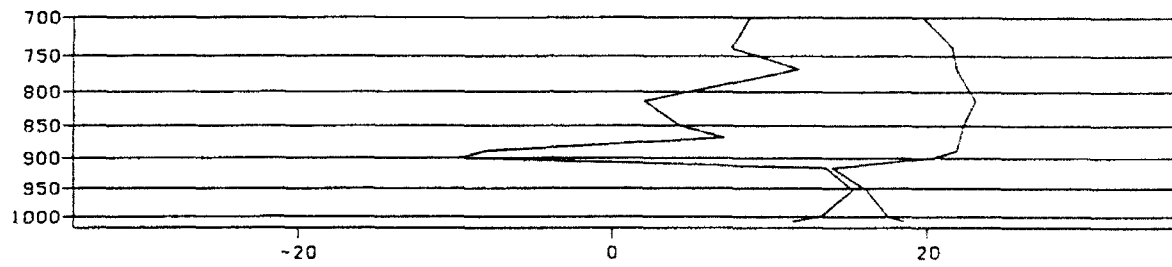


Figure 4: Temperature and dewpoint profile on a Skew-T Log P diagram showing an example of a complex moisture structure above the subsidence inversion in the eastern Atlantic Ocean.

Chapter 2

Data Used

The data used for this study are conventional upper air soundings from Lajes Air Base, Portugal on the island of Terciera in the Azores (Figure 5). Lajes is the only upper air reporting station located near the subtropical anticyclone in the eastern Atlantic. The data were obtained from the United States Air Force Environmental Technical Applications Center climatic database at the National Climate Data Center in Asheville, North Carolina. Parameters included were temperature, dewpoint, wind speed and wind direction for the surface, mandatory and significant pressure levels. These data were read into GEMPAK (General Meteorological Package) which was developed by the National Aeronautics and Space Administration at Goddard Space Flight Center, MD (desJardins et al., 1991). Within GEMPAK, parameters such as mixing ratio, potential temperature, equivalent potential temperature, etc., were obtained and analyzed. Inversion strength was also calculated and was defined as the magnitude of the difference between the potential temperature at the top of the subsidence inversion and the potential temperature at the base

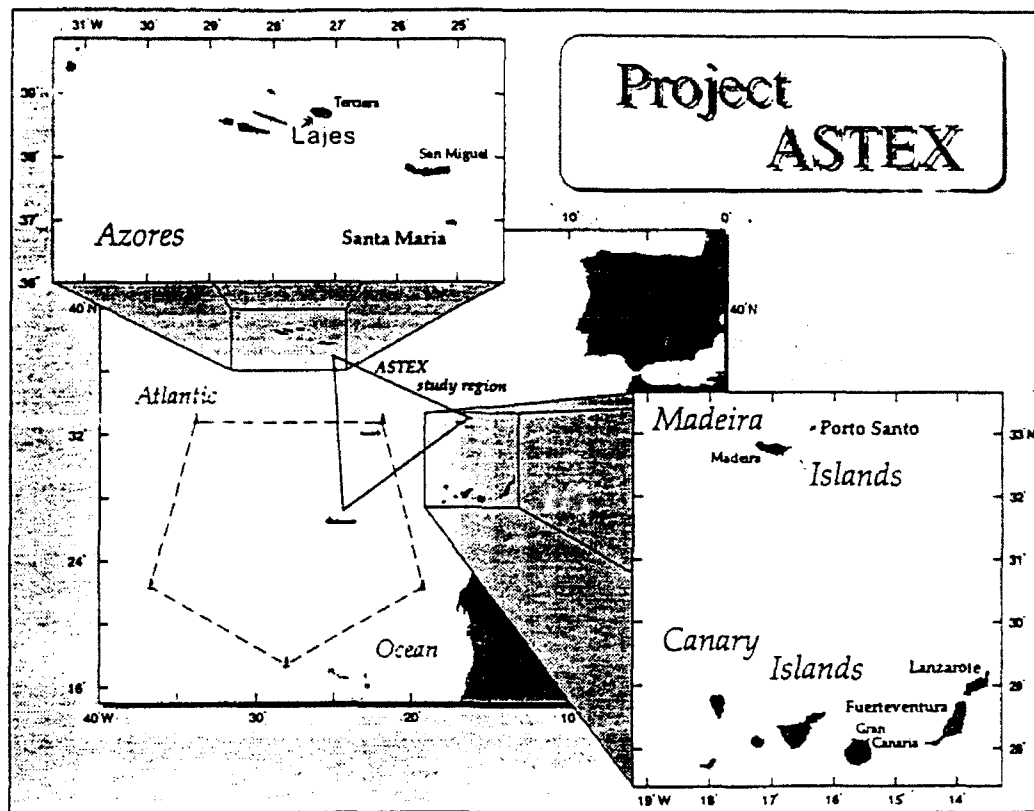


Figure 5: Map of ASTEX study area in the eastern Atlantic Ocean (FIRE Project Office and ASTEX Working Group, 1992).

of the subsidence inversion, divided by the pressure depth (in millibars) of that inversion. Calculating inversion strength provides a qualitative parameter which can be used to compare the characteristics of individual subsidence inversions. Inversion strength will also help to determine if the moist nose is created by moisture penetrating through the subsidence inversion via convective transport from the boundary layer. Calculated inversion strength is similar to a parameter used in ECMWF (European Center for Medium-range Weather Forecasting) climate models when parameterizing cloudiness below 750 mb (Sommeria et al., 1985).

The soundings used for this study were obtained from 1980 to 1990 for the month of June. Soundings were examined below 700 mb because moist noses over the subsidence inversions in the Pacific were located below 700 mb (Kloesel, 1992). Soundings were also examined below 700 mb to locate any features above the subsidence inversion and below 700 mb that may influence the subsidence inversion and boundary layer. Soundings which provided little or no information about the temperature and moisture structure from the surface to 700 mb were not considered. In addition, soundings with mandatory level information only or excessive missing data were eliminated. Soundings from the 29th and 30th of June were excluded from this study so that weekly averages would contain the same number of potential soundings for the same time period each year.

After the soundings with excessive missing data were eliminated during the initial examination of the data, 442 soundings remained. These soundings were divided into soundings with inversions and soundings without inversions. Soundings with inversions were then divided into three categories: soundings with subsidence inversions, soundings with frontal

inversions and soundings with inversions, but questionable data. These subdivisions will be defined in the next chapter. Soundings with subsidence inversions were then divided into soundings with a moist nose present above the subsidence inversion and soundings without a moist nose above the subsidence inversion to examine the thermodynamic structures of each and note any similarities or differences. Parameters from these two categories were further divided into 00 UTC and 12 UTC categories to examine diurnal variations, and into weekly categories to examine variations within the month of June. Week 1 corresponds to 1-7 June, Week 2 corresponds to 8-14 June, Week 3 corresponds to 15-21 June, and Week 4 corresponds to 22-28 June. Most of the standard meteorological variables, i.e. pressure, temperature, height, dewpoint, etc. were available with the exception of wind speed and direction, which only appeared to be reliable in approximately 10% of the soundings at the levels of interest (i.e. inversion base, inversion top, and the level at which the moist nose was present).

To compliment the data from Lajes, sounding data were also obtained from Funchal, located on the island of Madeira, and LaCoruña, Spain. However, it was determined by inspection that severe problems and inconsistencies were apparent in this data; therefore, these data were not used.

Chapter 3

Subsidence Inversion Climatology

3.1 Evidence of the Subsidence Inversion

The Lajes radiosonde data were used to study the vertical thermodynamic structure of Atlantic subsidence inversions because of its proximity to the climatological center of the Atlantic subtropical anticyclone. Figure 6 shows the mean sea level pressure pattern in the Atlantic Ocean during the month of June for 1980-1990. Based on this pattern, it is expected that all inversions during this period at Lajes are subsidence inversions. However, a time series plot of the daily surface pressure at Lajes during June, 1980 (Figure 7), reveals that the subtropical anticyclone is not as permanent a feature as is shown in Figure 6. The other ten years of data used for this study revealed similar daily pressure fluctuations for the month of June. Because of the transient nature of the anticyclone in the Atlantic, each sounding was analyzed individually to determine if a subsidence inversion was present.

Of the 442 soundings available, 361 soundings (81.7%) were identified as having an

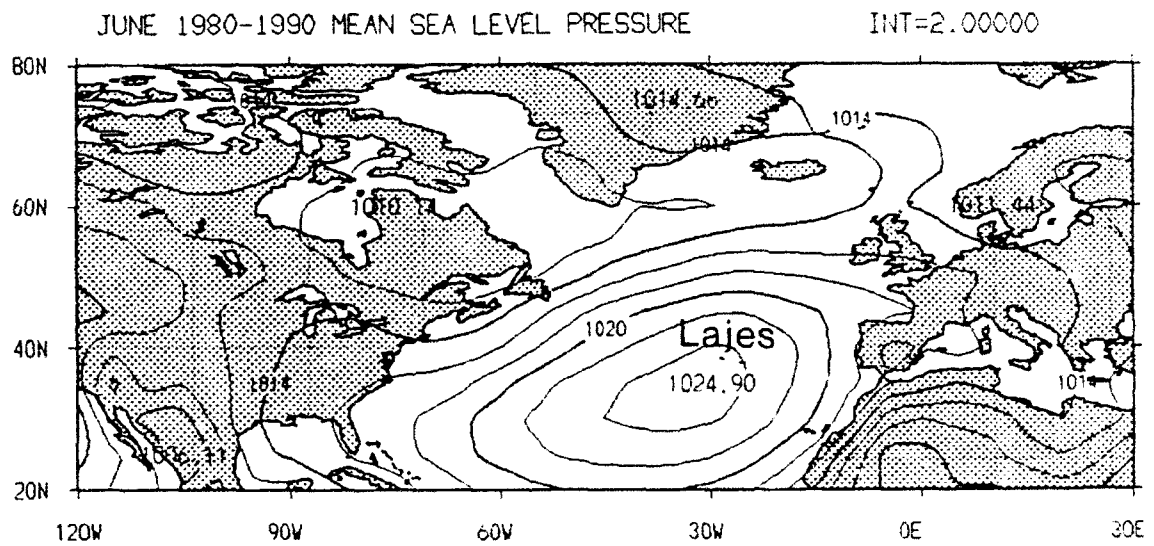


Figure 6: Mean sea level pressure plot of the Atlantic Ocean depicting the mean position and intensity of the subtropical anticyclone for the month of June, 1980-1990.

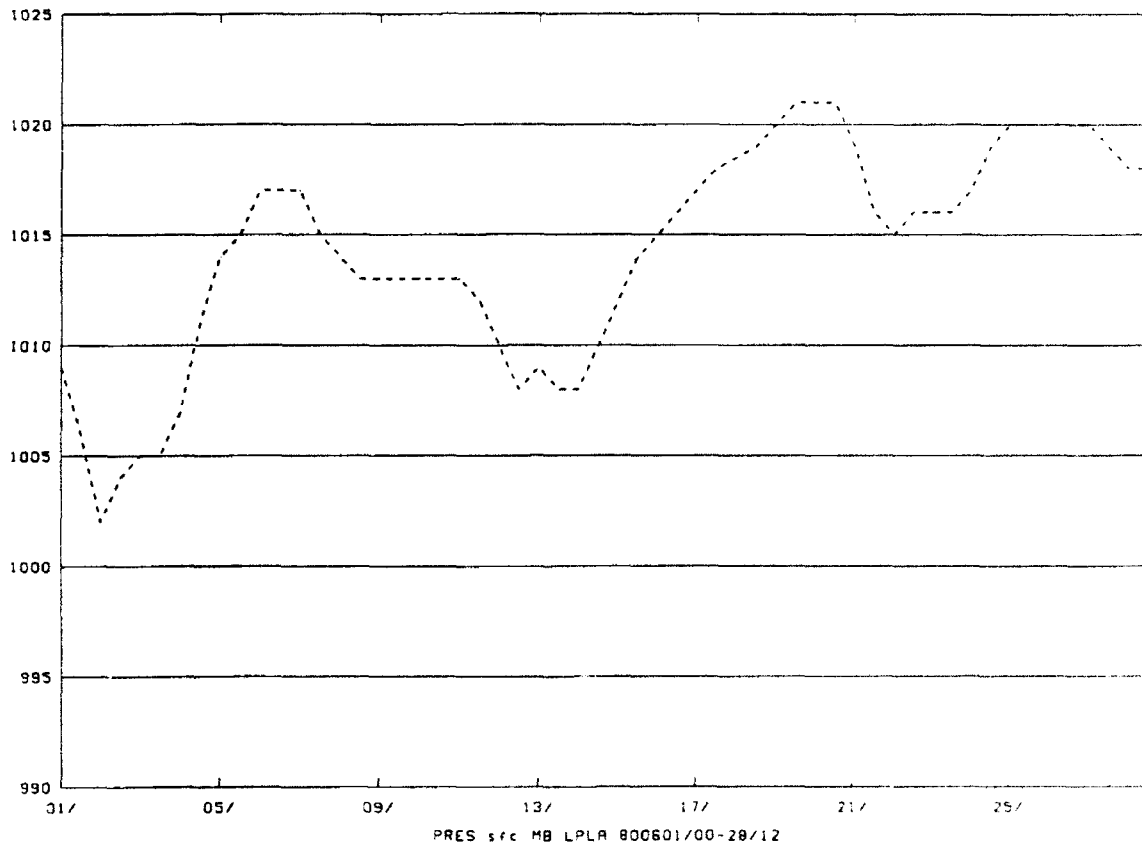


Figure 7: Time series plot of surface pressure for June 1980. Fifty-three data points were available for this year.

inversion present above a finite surface boundary layer. The boundary layer was determined as the part of the troposphere that is directly influenced by the earth's surface, which responds to surface forcings within a timescale of an hour or less (Stull, 1988). An indication of subsidence occurring within the inversion would be drying within the inversion. Figure 8 shows a histogram of the difference between the mixing ratio at the base of the inversion and the mixing ratio at the top, with negative values indicating drying. (Note: the number of inversions to the right of the '0' column have values of $\Delta q \geq 0$.) Overall, 302 of the 361 soundings (83.7%) with inversions exhibited drying within the inversion. Figure 9 shows a plot of the mean temperature and mixing ratio at the surface, inversion base and inversion top for soundings that exhibit drying within the inversion. This profile is typical of a "classic" subsidence inversion (HQ, Air Weather Service, 1961).

The remaining 59 soundings in which drying did not occur were also examined in detail. Twenty-five soundings contained inversions associated with frontal systems moving through Lajes, so these were removed from the analysis of subsidence inversions. Four soundings contained layers with superadiabatic lapse rates that gave a false impression that an inversion was present in the sounding. An example is shown in Figure 10(a). Since no techniques could be employed to smooth the effects of the superadiabatic lapse rates in the soundings, the soundings were removed from the analysis of subsidence. Five additional soundings were also categorized as having unreliable data. An example of these is shown in Figure 10(b). These five were also removed from the analysis of subsidence. Three soundings showed subsidence inversions in which moisture may have subsided into the inversion layer. Figure 10(c) shows one of the soundings in which this occurred. Note that the winds in this

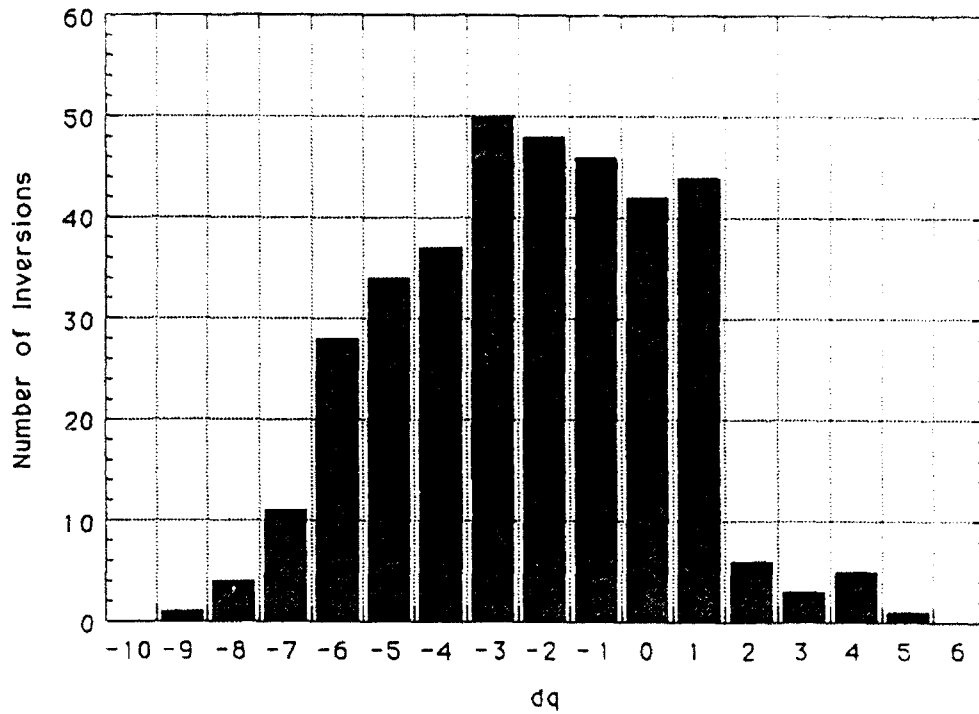


Figure 8: Histogram of the difference of mixing ratio between the top and bottom of the inversion. (in g/kg). Negative values indicate drying within the inversion. The number of inversions to the right of the '0' column have values of $\Delta q \geq 0$.

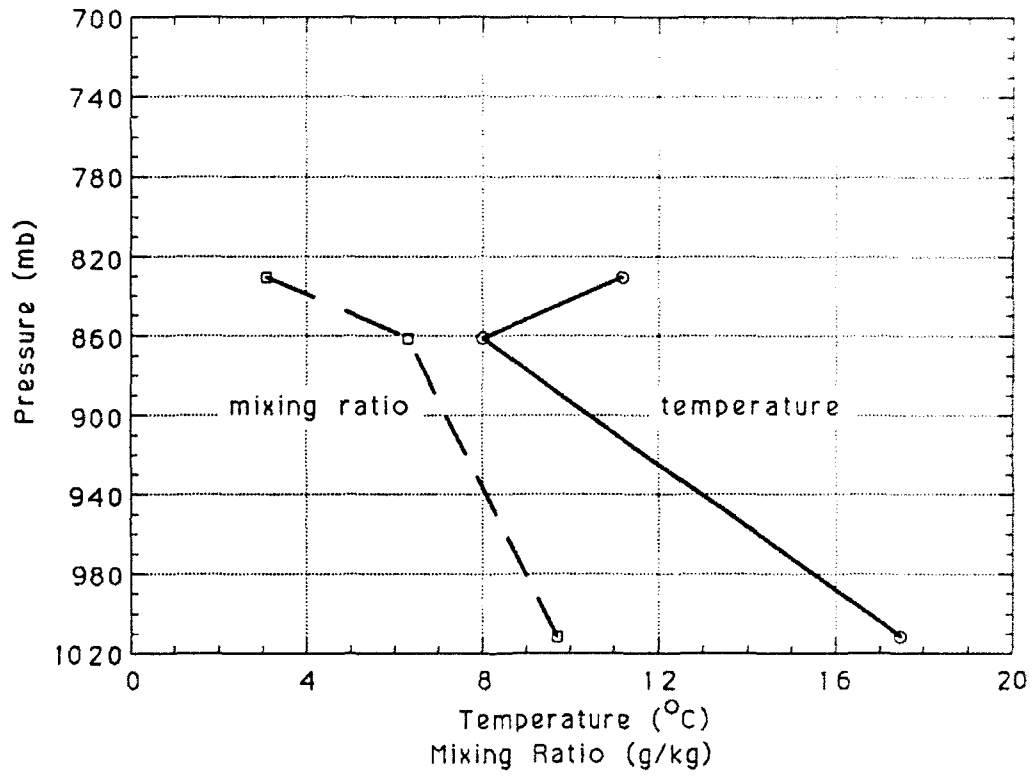
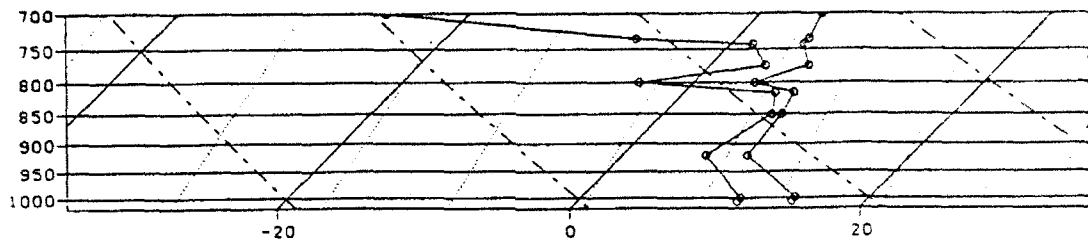
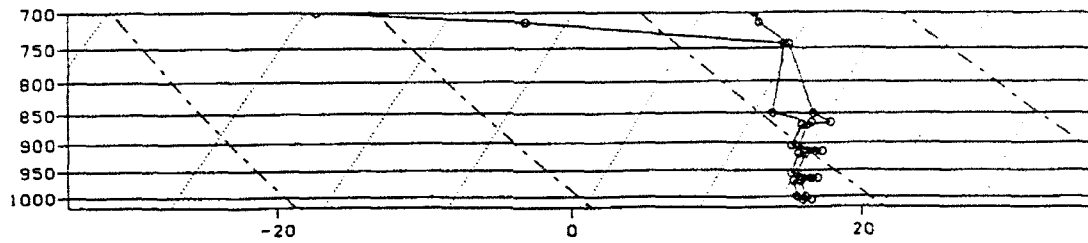


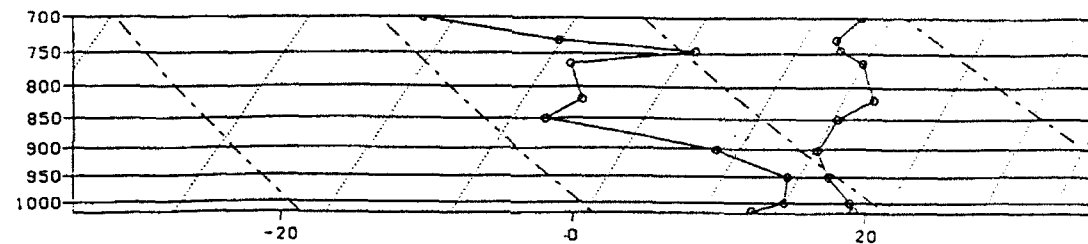
Figure 9: Mean plot of temperature and mixing ratio at the surface, inversion base and inversion top for all soundings with subsidence inversions for Lajes in June 1980-1990.



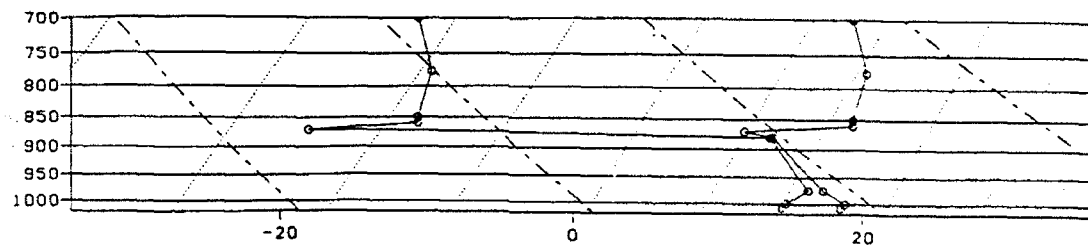
(a)



(b)



(c)



(d)

Figure 10: Skew T Log P diagrams depicting temperature and dewpoint profiles of (a) a sounding containing a superadiabatic lapse rate, (b) an unreliable sounding, (c) a sounding in which moisture may have subsided into the inversion, and (d) a subsidence inversion in which the appearance of moisture increase within the inversion was due to the 30° C maximum dewpoint depression coding convention.

sounding were light and variable from the surface to 700 mb, indicating that the center of the anticyclone, and the strongest subsidence, was located over Lajes. The location of the subtropical anticyclone for this sounding was verified with a surface map for the same time. This same pattern is true of the other two cases as well. Subsidence inversions were present in the soundings immediately preceding and following these three soundings, so these soundings were kept for the analysis. The remaining 22 soundings appeared to have increased absolute moisture within the inversion due to the 30° C maximum dewpoint depression coding convention when relative humidity is less than 21%. The dewpoint depressions within the inversions were, in all likelihood, greater than 30 degrees, but when the temperature increased in the inversion, so did the dewpoint, thereby giving the impression that moisture increased from the base to the top of the inversion. Figure 10(d) shows an example of this. These soundings were classified as having subsidence inversions and were retained for the analysis of subsidence. Even though this introduces bogus mixing ratio values into the data set, the 22 soundings represent only 6.7% of the total number of soundings used for the analysis of subsidence.

The next section will present information about the climatology of all subsidence inversions identified in the Lajes data set to gain an understanding of the mean profile of temperature and mixing ratio of the marine boundary layer and subsidence inversion.

3.2 Thermodynamic Structure of the Subsidence Inversion

The mean profiles of boundary layer and inversion temperature and mixing ratio for the 327 soundings identified as having a subsidence inversion can be seen in Figure 11 and Figure 12, respectively. Again, the layer of increasing temperature in Figure 11 denotes the base and top of the inversion, and the corresponding mixing ratio profile in Figure 12 shows drying within the inversion. These factors, as well as the synoptic conditions observed in the region (Figure 6), indicate subsidence is the dominant feature of the inversions in this region. The mean temperature and mixing ratio at the surface are 17.5°C and 9.7 g/kg respectively ($\text{RH} = 77\%$). The mean pressure level of the subsidence inversion base is 861 mb (1481 m). The mean temperature and mixing ratio at the base of the subsidence inversion are 8.0°C and 6.3 g/kg , respectively ($\text{RH} = 79\%$). The mean pressure of the top of the subsidence inversion is 831 mb (1783 m). The mean temperature and mixing ratio at the top of the subsidence inversion are 11.2°C and 3.1 g/kg , respectively ($\text{RH} = 30\%$). The mean inversion strength of the subsidence inversions studied is 0.257 K/mb ($1.06^{\circ}\text{C}/100\text{ m}$). Figure 13 shows the mean potential temperature profile for all soundings with subsidence inversions. This profile is characteristic of a stable boundary layer, which is consistent with the knowledge that marine stratocumulus regimes are stable boundary layer regimes.

Figures 11 and 12 also show the diurnal variation of the temperature and mixing ratio at the same levels. The main point to note is that the 12 UTC (local time at Lajes is UTC - 1) mean surface temperature is 18.0°C , or 1.0°C higher than the 00 UTC mean surface temperature of 17.0°C . This mean difference is due to normal daytime surface heating.

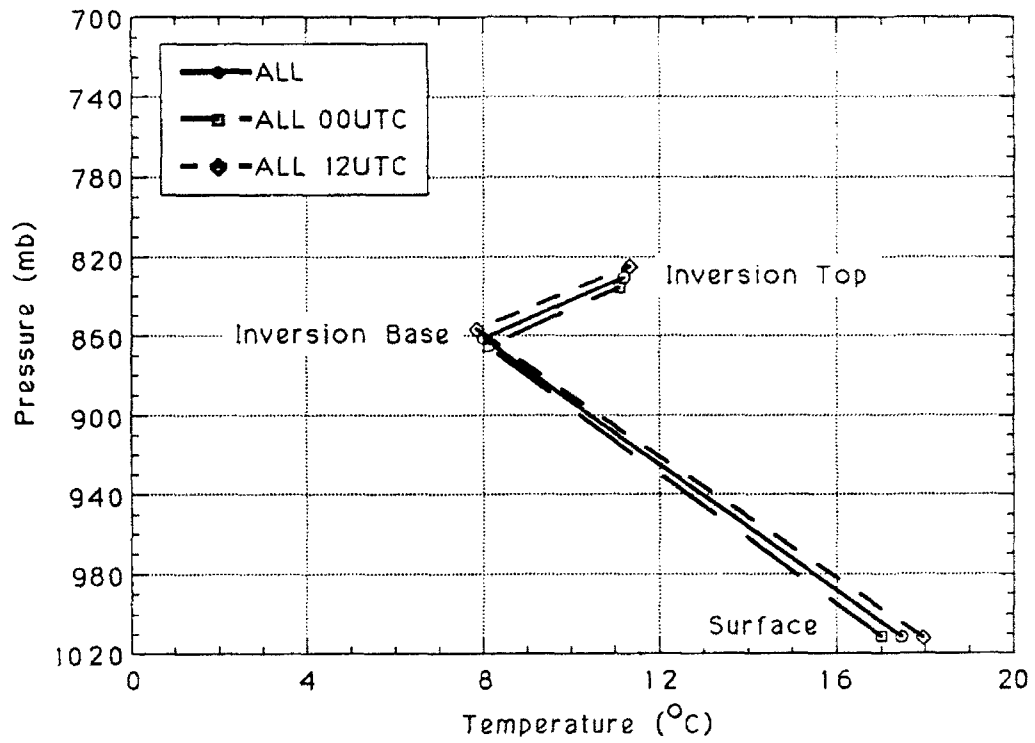


Figure 11: Mean temperature profile of boundary layer and subsidence inversion for all times (solid line), 00 UTC (long dash), and 12 UTC (short dash).

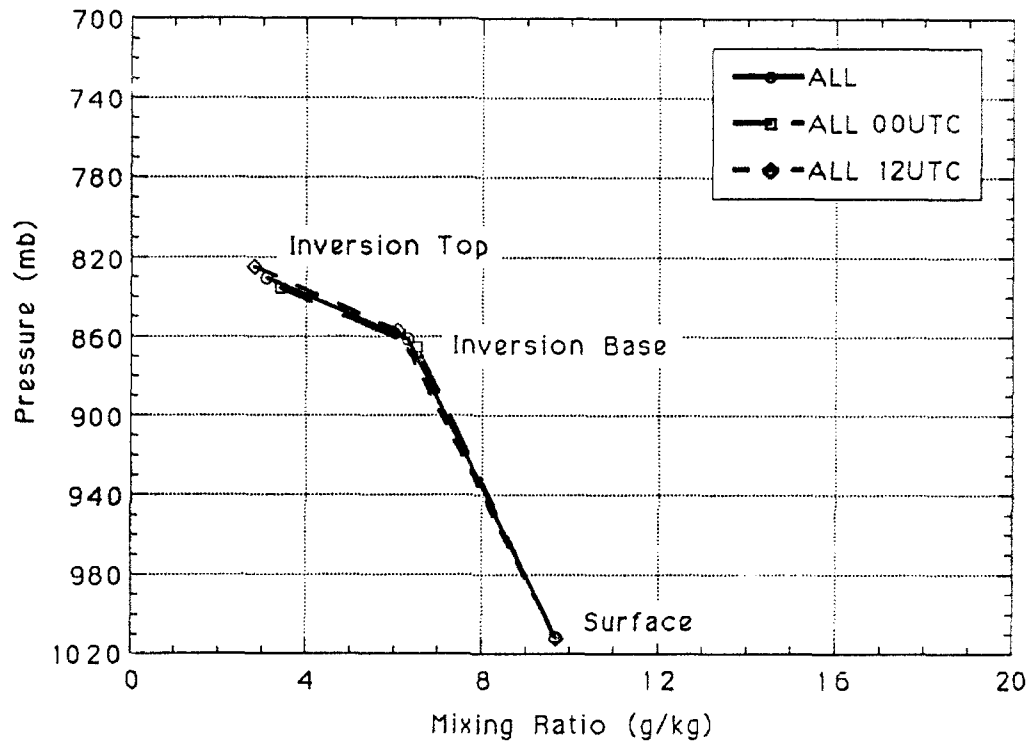


Figure 12: Mean mixing ratio profile of boundary layer and subsidence inversion for all times (solid line), 00 UTC (long dash), and 12 UTC (short dash).

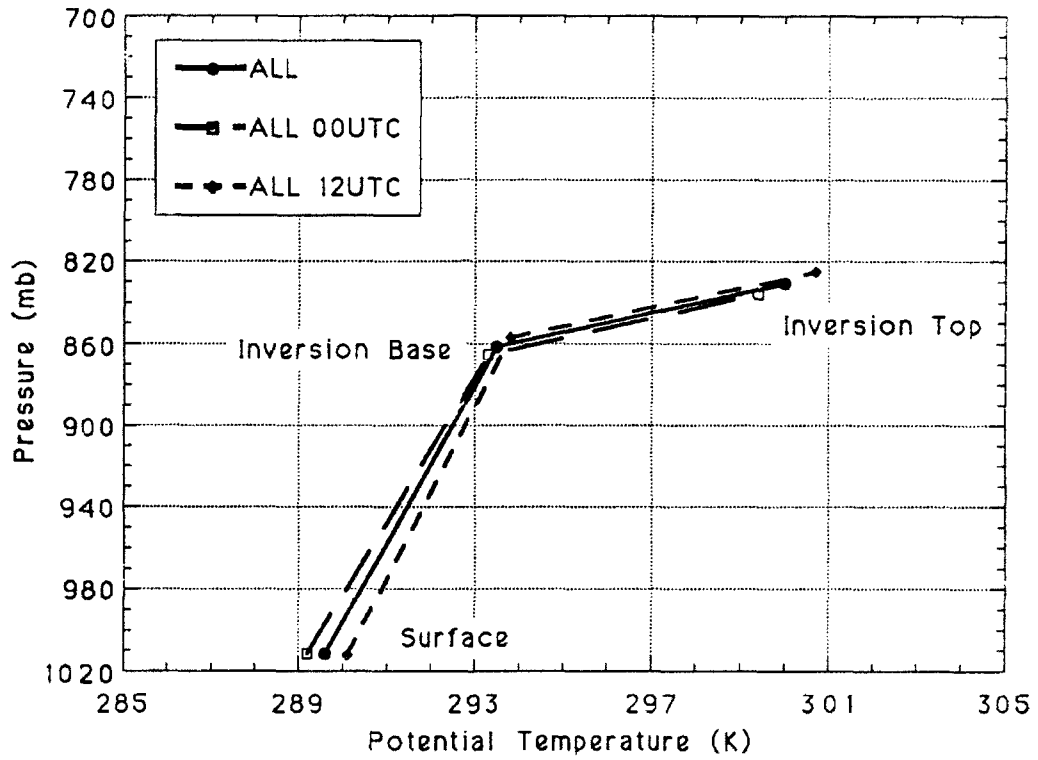


Figure 13: Mean potential temperature profile of boundary layer and subsidence inversion for all times (solid line), 00 UTC (long dash), and 12 UTC (short dash).

The mean mixing ratio at the surface is 9.7 g/kg at 00 UTC and at 12 UTC. The mean relative humidity at 00 UTC is 77%, which decreases to 74% at 12 UTC.

The mean inversion base pressure at 00 UTC is 866 mb (1431 m) and decreases 9 mb (increases 105 m) by 12 UTC. If one were to assume that mixing increases in the boundary layer during the day, an increase in the surface temperature by 1.0° C during the day would result in a 10 mb rise in the inversion base pressure through heating of the boundary layer. This value is consistent with the findings above.

The mean inversion base temperature and mixing ratio at 00 UTC are 8.1° C and 6.5 g/kg, respectively, and both values lower to 7.8° C and 6.1 g/kg, respectively, at 12 UTC. The mean relative humidity decreases from 80% at 00 UTC to 77% at 12 UTC. The mean boundary layer lapse rates are 6.9° C/km at 00 UTC and 7.2° C/km at 12 UTC. The increase in lapse rate is also due to surface heating during the day.

The mean inversion top pressure at 00 UTC is 836 mb (1725 m) and decreases 11 mb (increases 120 m) by 12 UTC. The mean inversion top temperature and mixing ratio at 00 UTC are 11.2° C and 3.4 g/kg, respectively (RH = 33%). The mean mixing ratio at the top of the subsidence inversion lowers to 2.8 g/kg by 12 UTC, but the mean temperature at the top of the subsidence inversion increases just slightly to 11.3° C (RH = 26%). This slight increase in temperature may be caused by increased subsidence at 12 UTC, but it is not known whether there is a diurnal cycle associated with the subsidence. The mean inversion strength also increases slightly from 00 UTC (0.257 K/mb, 1.05° C/100 m) to 12 UTC (0.260 K/mb, 1.13° C/100 m). The slight strengthening by 12 UTC may account for the increase in temperature at the top of the subsidence inversion.

Diurnal variations in the subsidence inversion have been examined to understand the effects of daytime heating on mixing in the boundary layer and on variations in the subsidence inversion. To understand the seasonal variations of the marine boundary layer and the subsidence inversions, weekly means were calculated (discussed in Chapter 2).

Figures 14 and 15 show the mean weekly values of temperature and mixing ratio, respectively, for all the soundings with a subsidence inversion. The mean surface temperature increases from 16.7° C in Week 1 to 17.1° C in Week 2 and 18.1° C in Week 3, but decreases slightly to 17.8° C in Week 4. This is climatologically consistent with the temperature increase observed as summer approaches, except for the slight decrease in Week 4. The mean mixing ratio at the surface is about 9.2 g/kg in Week 1 and increases to 9.6 g/kg in Week 2, then increases again to 10.1 g/kg in Week 3, then decreases slightly in Week 4 to 9.8 g/kg. The relative humidity is around 77% all four weeks.

The inversion base pressure varies from 860 mb (1485 m) in Week 1 to 847 mb (1582 m) in Week 2, then to 871 mb (1429 m) in Week 3 and 867 mb (1448 m) in Week 4. The mean temperature of the subsidence inversion base increases by 2.5° C from 7.0° C in Week 1 to 9.5° C in Week 3, but decreases by 1.4° C to 8.2° C in Week 4. The mean weekly mixing ratio at the base of the subsidence inversion is 6.0 g/kg for Weeks 1 and 2 with a 0.7 g/kg increase to 6.7 g/kg in Week 3 and a decrease to 6.2 g/kg in Week 4. The relative humidity in Week 1 is 82% and decreases to 77% in Weeks 2 through 4.

The subsidence inversion top pressure is 830 mb (1787 m) in Week 1, decreases to 817 mb (1874 m) in Week 2, increases to 840 mb (1735 m) in Week 3, then decreases again to 834 mb (1754 m) in Week 4. The mean temperature at the top of the subsidence inversion follows

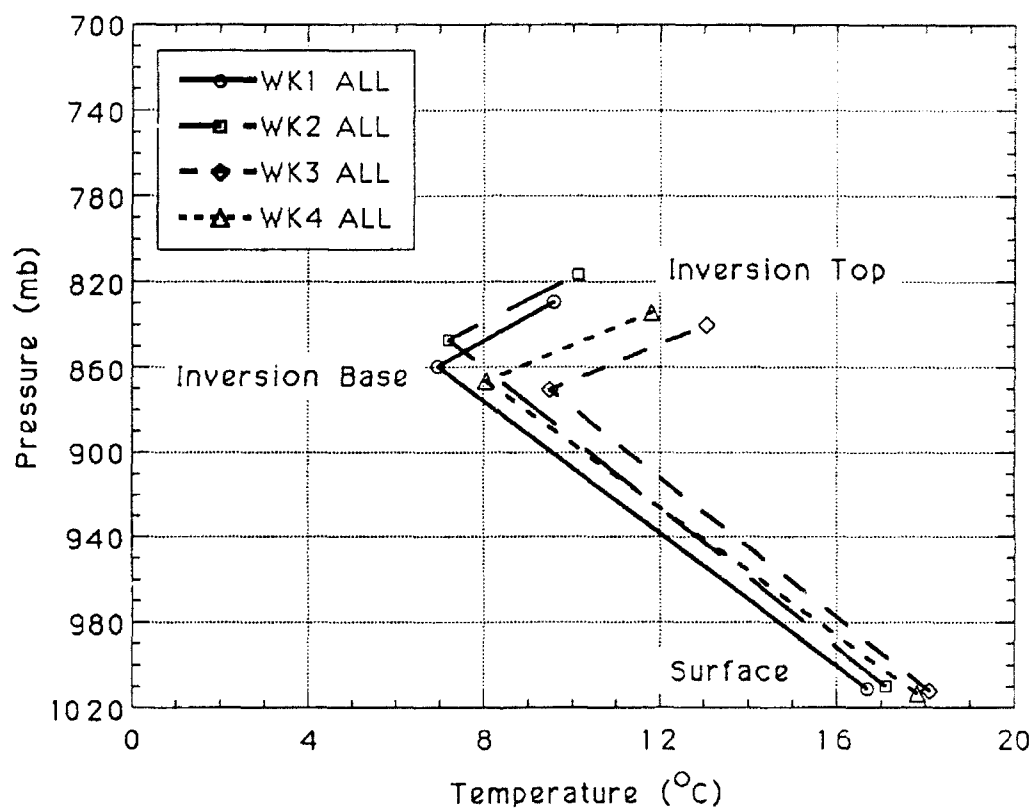


Figure 14: Mean weekly temperature profile of the boundary layer and subsidence inversion. Each week is indicated as follows: Week 1, solid line; Week 2, long dash; Week 3, medium dash; Week 4, short dash.

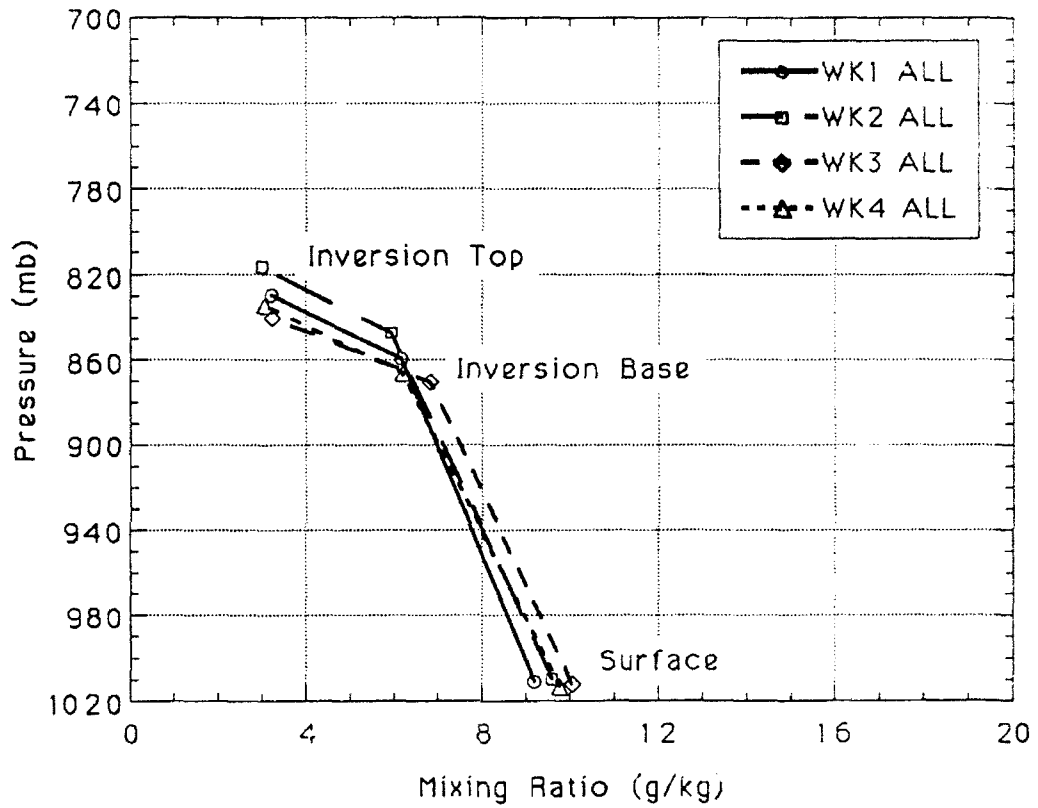


Figure 15: Mean weekly mixing ratio profile of the boundary layer and subsidence inversion. Each week is indicated as follows: Week 1, solid line; Week 2, long dash; Week 3, medium dash; Week 4, short dash.

a similar pattern in that it increases by 3.5°C from 9.6°C in Week 1 to 13.1°C in Week 3, but decreases by 1.3°C to 11.8°C in Week 4. The mean mixing ratio at the subsidence inversion top is 3.2 g/kg in Week 1, 3.0 g/kg in Week 2, 3.2 g/kg in Week 3, and 3.1 g/kg in Week 4. The relative humidity in Week 1 is 35%, decreases to 30% in Week 2, then decreases slightly to 28% in Week 3, and slightly increases to 29% in Week 4.

Figure 16 shows the mean weekly inversion strength for all soundings with subsidence inversions. The results indicate a gradual strengthening of the subsidence inversions from 0.229 K/mb ($0.86^{\circ}\text{C}/100\text{ m}$) in Week 1 to 0.277 K/mb ($1.18^{\circ}\text{C}/100\text{ m}$) in Week 4, even as the surface temperature, on average, is increasing. This structure appears to reflect the onset of the establishment of the Atlantic subtropical anticyclone. To support this, the time series plot of daily surface pressure in Figure 7 will be used here. This daily plot of surface pressure exhibits a general upward trend, although the transience of the high is evident. This same trend can be seen in 1981, 1983, 1985, and 1986 (not shown). However, no significant upward trend could be seen in the surface pressure plots for 1984, 1989, or 1990. (1982 and 1987 only had 9 and 19 data points to plot, respectively. The other years all had at least 40 out of a possible 56 data points plotted.) That some years exhibit the upward trend and some do not may explain the weekly variability discussed above.

The mean marine boundary layer and subsidence inversion profiles have been examined to better understand the thermodynamic structure associated with the subtropical anticyclone as well as how the thermodynamic structure varies diurnally and weekly during the month of June. The diurnal variations of surface and subsidence inversion base and top variables behaved in a generally predictable manner. However, the weekly variations of the

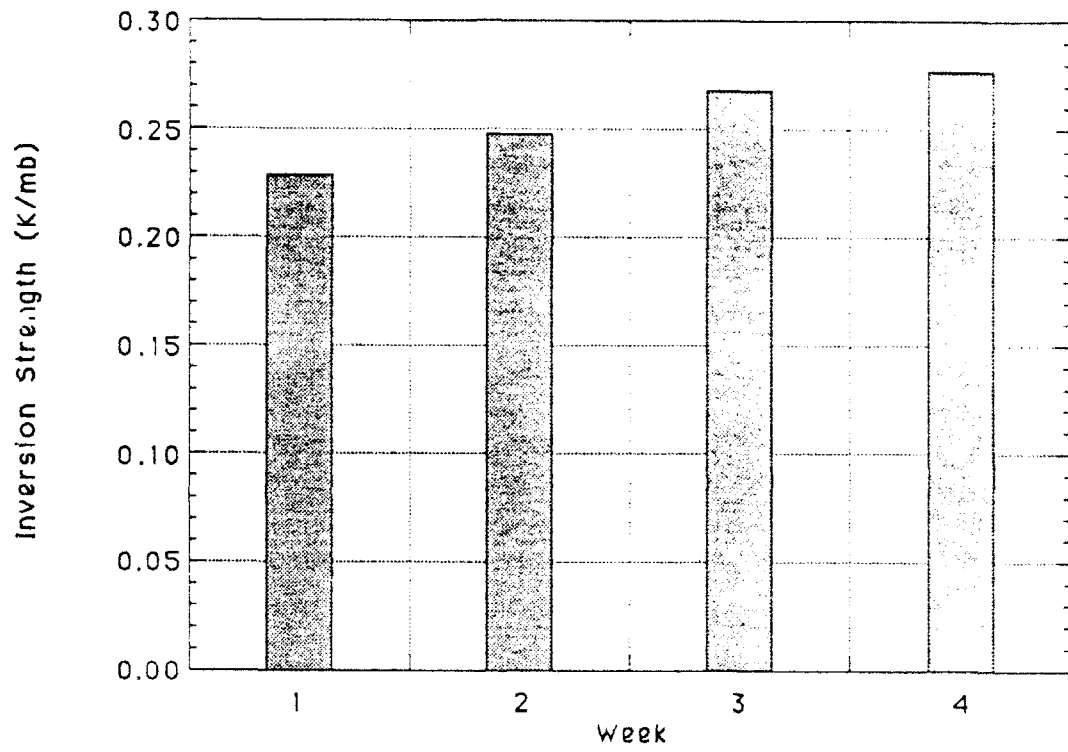


Figure 16: Mean weekly inversion strength (K/mb) for soundings with subsidence inversions.

variables shown did not show any predictable pattern, possibly due to the transience of the subtropical anticyclone and how, on a weekly basis, the overall synoptic pattern differs from year to year. The next chapter will examine how the thermodynamic structure differs between subsidence inversions with and without a moist nose present.

Chapter 4

Above-Subsidence Inversion

Structure

As stated in Chapter 1, there is evidence of a complex moisture structure above the subsidence inversion. Edinger (1963) first documented the presence of the moist layer above the subsidence inversion over the marine stratocumulus clouds off the California coast, but concluded that the moist layer was caused by detrainment from convective turrets that had penetrated the inversion. Lilly (1968) also noted the presence of the moist layer, but dismissed it as instrument error. A time series plot of temperature and specific humidity profiles observed over the Atlantic during ATEX illustrates another example of this complex moisture structure (Figure 17, Augstein et al., 1974). This moisture profile structure above the inversion is more complex than the one currently parameterized in marine boundary layer and climate models (e.g. Figure 2 from Chapter 1).

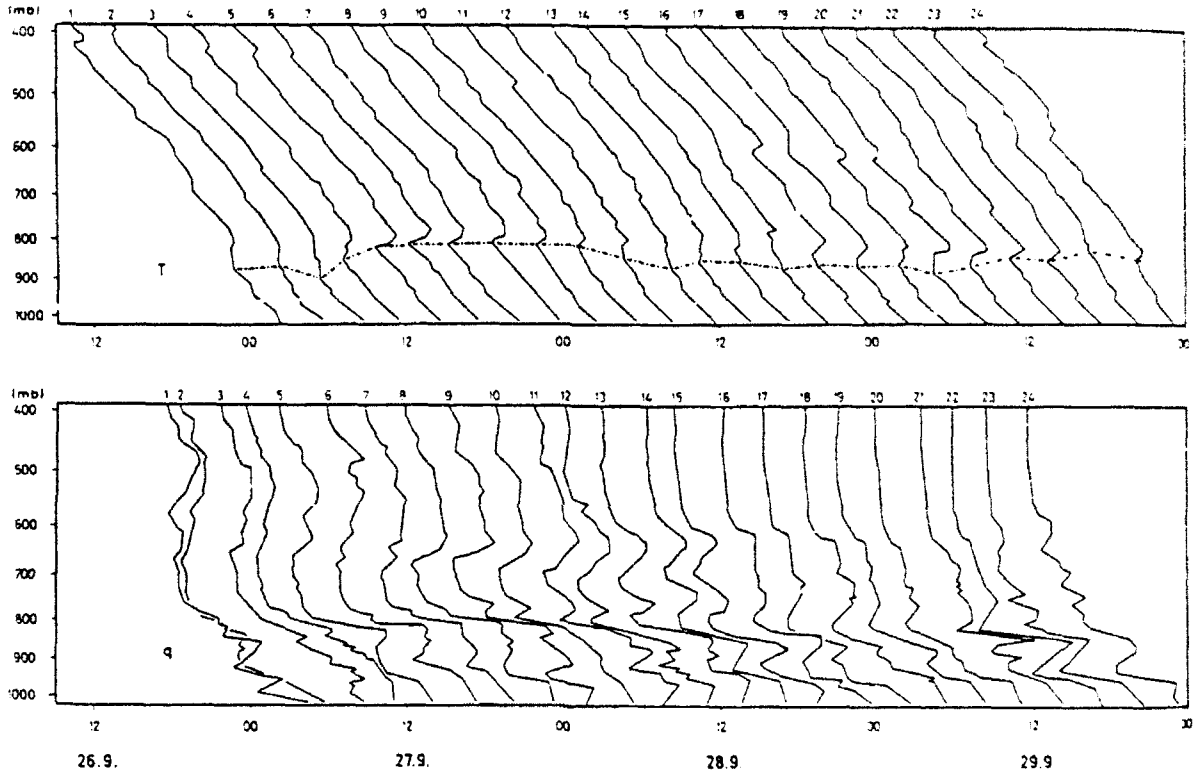


Figure 17: Time series plot of temperature (T) and specific humidity (q) taken during ATEX on 26-29 September 1969 at 30°W/0°N (from Augstein et al., 1974).

Similar complex moisture profiles were discovered in the Lajes radiosonde data. Of the 327 soundings with a subsidence inversion, 129 (39.4%) had an identifiable moist nose present above the subsidence inversion similar to the example seen in Figure 4 from Chapter 1. The high frequency of occurrence of this feature warrants a more thorough analysis. Therefore, this chapter will provide information about the climatology of the moist nose and examine the thermodynamic structure of the subsidence inversions with moist noses and subsidence inversions without moist noses in order to evaluate Edinger's hypothesis. A comparison of the cases with moist noses to those without will provide information about the similarities and differences between the thermodynamic structures associated with each.

4.1 Climatology of Subsidence Inversions With Moist Nose Structure

The mean pressure of the moist nose in the soundings studied is 792 mb (2208 m), which is 65 mb lower (689 m higher) than the mean pressure of the top of subsidence inversions which have moist noses present. The mean temperature in the moist nose layer is 9.2° C, which is 3.3° C lower than the mean temperature at the top of the subsidence inversions with a moist nose. The mean mixing ratio in the moist nose is 5.5 g/kg, 1.7 g/kg (24%) higher than the mean mixing ratio at the top of subsidence inversions with a moist nose. The mean relative humidity of the moist nose is 58%.

Mean profiles of temperature and mixing ratio at the surface, inversion base and inversion top for subsidence inversions with moist noses present are shown in Figures 18 and 19.

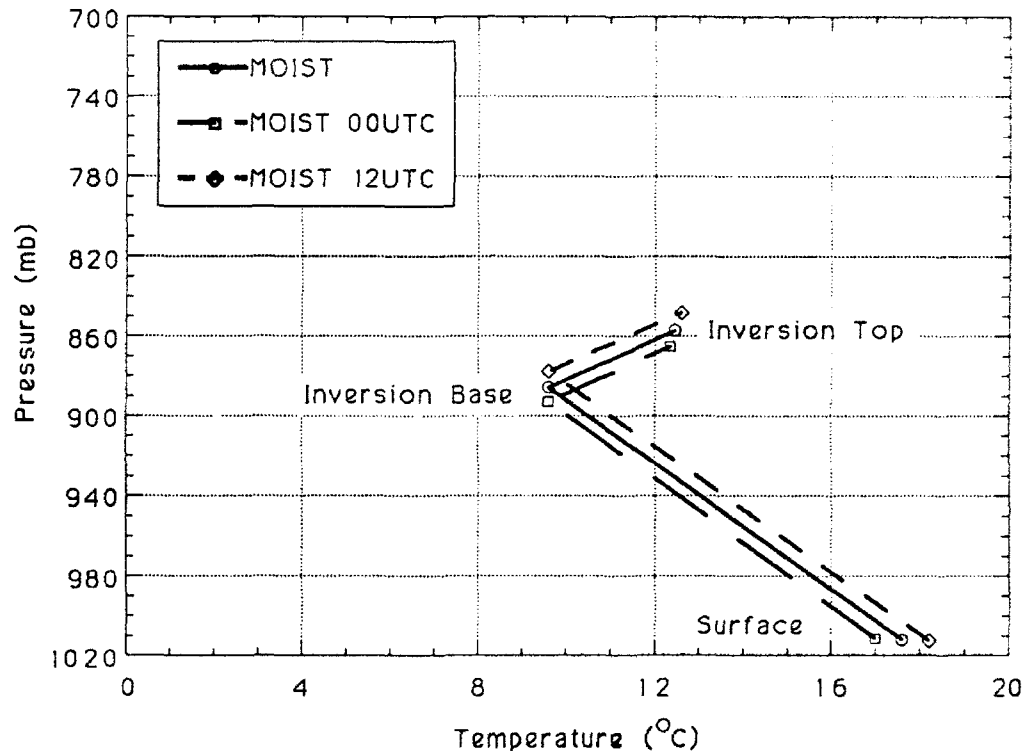


Figure 18: Mean temperature profile of boundary layer and inversion for all subsidence inversions with a moist nose present for all times (solid line), 00 UTC (long dash), and 12 UTC (short dash).

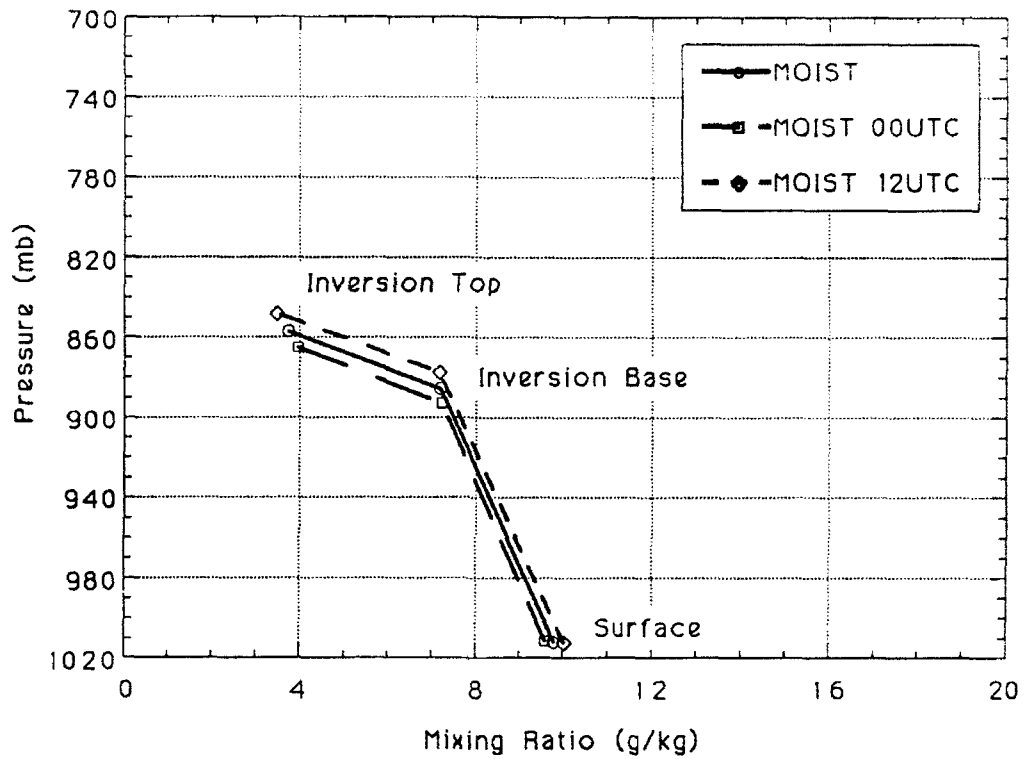


Figure 19: Mean mixing ratio profile of boundary layer and inversion for all subsidence inversions with a moist nose present for all times (solid line), 00 UTC (long dash), and 12 UTC (short dash).

The mean temperature and mixing ratio at the surface are 17.6°C and 9.8 g/kg , respectively ($\text{RH} = 77\%$). The mean pressure of the base of the subsidence inversion with a moist nose present is 886 mb (1255 m). The mean temperature and mixing ratio at the base of the subsidence inversion are 9.6°C and 7.2 g/kg , respectively ($\text{RH} \approx 83\%$). The mean pressure of the top of the subsidence inversion is 857 mb (1538 m). The mean temperature and mixing ratio at the top of the subsidence inversion are 12.5°C and 3.8 g/kg , respectively ($\text{RH} = 35\%$). The mean inversion strength for subsidence inversions with a moist nose present is 0.227 K/mb ($1.02^{\circ}\text{C}/100\text{ m}$).

In order to better understand when these moist layers occur, diurnal variations of the moist nose were examined. At 00 UTC, 40.4% of the subsidence inversions analyzed had moist noses. The percentage decreases slightly to 38.5% at 12 UTC. The mean pressure of the moist nose at 00 UTC is 796 mb (2180 m), which is 69 mb lower (714 m higher) than the mean pressure of the top of inversions which have moist noses present at 00 UTC. At 12 UTC, the mean pressure of the moist nose is 789 mb (2244 m), 59 mb lower (622 m higher) than the mean pressure of the top of inversions which have moist noses present at 12 UTC. The mean temperature and mean mixing ratio in the moist nose at 00 UTC are 9.1°C and 5.6 g/kg , respectively. The mean relative humidity in this layer at 00 UTC is 60%. The mean temperature at 12 UTC increases to 9.4°C , while the mixing ratio decreases slightly to 5.4 g/kg . This corresponds to a slight decrease in the relative humidity to 56% at 12 UTC.

Diurnal variations of surface temperature and surface mixing ratio associated with soundings which exhibit the moist nose structure are similar to the diurnal variations from

all soundings with subsidence inversions presented in Chapter 3. The mean surface temperature increases from 17.0° C at 00 UTC to 18.3° C at 12 UTC. Again, this mean difference is due to normal daytime heating at the surface. The mean surface mixing ratio increases from 9.6 g/kg at 00 UTC to 10.0 g/kg at 12 UTC. The mean relative humidity is 79% at 00 UTC and decreases to 75% at 12 UTC.

Between 00 UTC and 12 UTC, the inversion base pressure decreases from 893 mb (1183 m) to 878 mb (1345 m), a 15 mb decrease (162 m increase). Again, if the assumption is made that mixing is occurring in the boundary layer during the day, then a 1.3° C increase in surface temperature would result in a 14 mb decrease in the inversion base pressure. This finding is consistent with the observed 15 mb decrease above.

The mean inversion base temperature and mixing ratio for subsidence inversions with a moist nose present are 9.6° C and 7.2 g/kg, respectively, at both 00 UTC and 12 UTC. The mean relative humidity at 00 UTC is 84% and decreases slightly to 81% at 12 UTC. It is interesting to note that although the base of the subsidence inversion is higher (by 15 mb) during the day in the moist nose cases, the mean temperature of the inversion base does not change.

The mean inversion top pressure for subsidence inversions with a moist nose present decreases from 865 mb (1466 m) at 00 UTC to 848 mb (1622 m) at 12 UTC. The mean inversion top temperature and mixing ratio at 00 UTC are 12.4° C and 4.0 g/kg, respectively (RH = 37%). The mean mixing ratio at the top of the subsidence inversion decreases to 3.5 g/kg at 12 UTC, but the mean temperature at the top of the subsidence inversion increases slightly to 12.6° C (RH = 31%) at 12 UTC. Similar trends were seen in the diurnal

variations of mean temperature and mixing ratio at the top of all subsidence inversions presented in Chapter 3. The mean inversion strength for the soundings with the moist nose at 00 UTC is 0.230 K/mb (1.08° C/100 m) and decreases slightly to 0.224 K/mb (0.99° C/100 m) by 12 UTC.

Weekly means of variables for subsidence inversions with moist noses were calculated to see if the onset of the anticyclone in the Atlantic has an influence on the moist noses. The weekly percentage of subsidence inversions with the moist nose present is depicted in Figure 20. There are 17-20% more inversions with the moist nose present in Week 3 than in Weeks 1, 2 and 4. The mean weekly pressure of the moist nose is 795 mb (2186 m) in Week 1, decreases to 785 mb (2220 m) by Week 2, then increases by Week 3 to 802 mb (2140 m), then decreases again to 783 mb (2306 m) by Week 4. The mean weekly temperature associated with the moist nose is 8.3° C in Week 1, 8.5° C in Week 2, 10.4° C in Week 3, and 8.9° C in Week 4. The mean mixing ratio varies only slightly from week to week to within ± 0.16 g/kg of 5.5 g/kg. The mean relative humidity of the moist nose is 62% in Weeks 1 and 2, then decreases to 55% in Week 3 and increases to 59% in Week 4.

The mean weekly temperature and mixing ratio profiles are shown in Figure 21 and 22, respectively, for subsidence inversions with moist noses. The mean weekly surface temperature increases from 16.9° C in Week 1 to 17.8° C in Week 2, then increases slightly to 18.0° C in Week 3, and decreases slightly to 17.9° C in Week 4. This trend is also seen in the mean surface temperature of all soundings with subsidence inversions. The mean weekly mixing ratio is 9.5 g/kg in Week 1 (RH = 79%), increases to 10.2 g/kg in Week 2 (RH = 81%), then decreases to 9.7 g/kg in Week 3 (RH = 76%), then increases

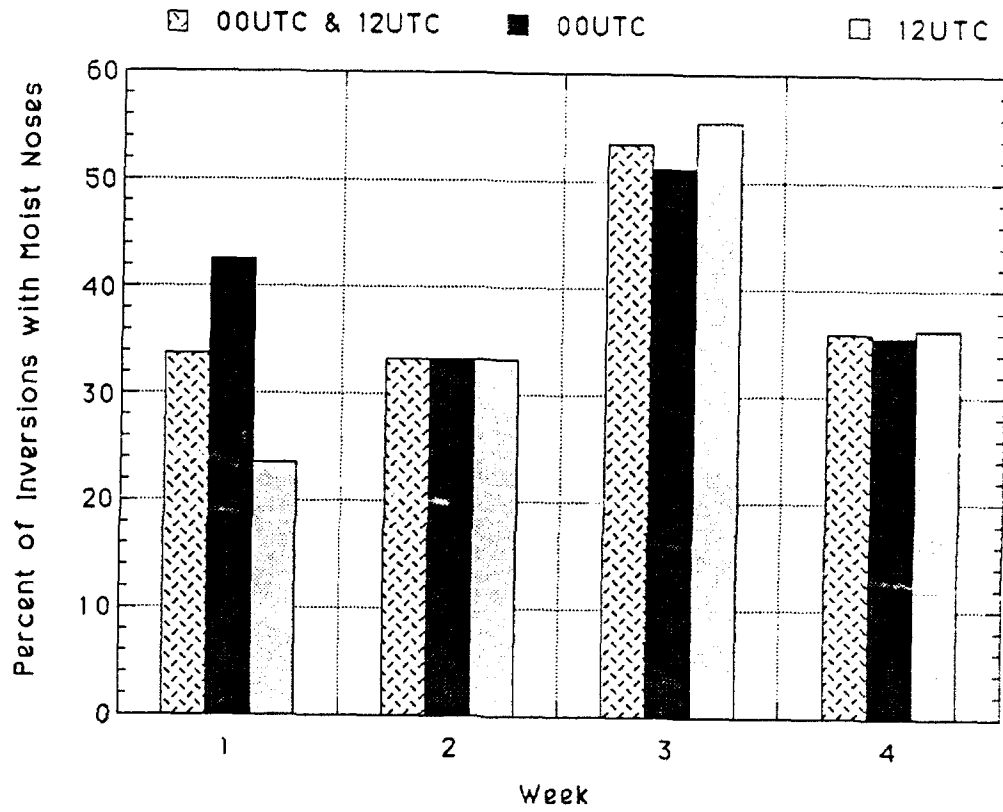


Figure 20: Weekly percentage of subsidence inversions with the moist nose present.

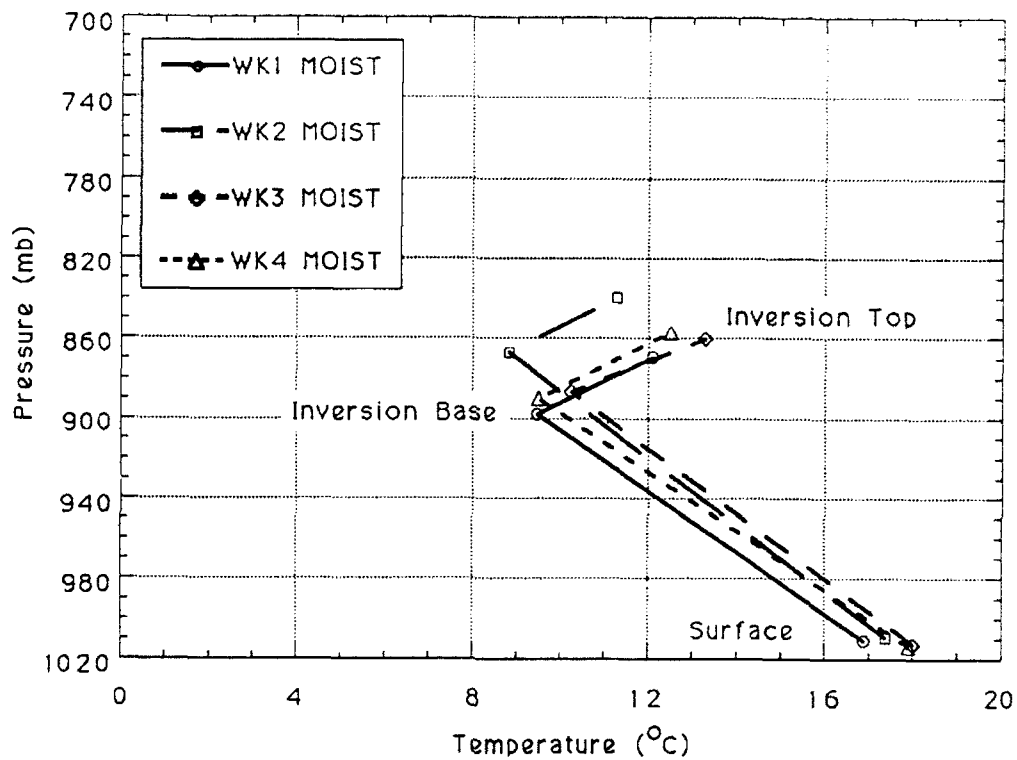


Figure 21: Mean weekly temperature profile of the boundary layer and inversion of subsidence inversions with moist noses. Each week is indicated as follows: Week 1, solid line; Week 2, long dash; Week 3, medium dash; Week 4, short dash.

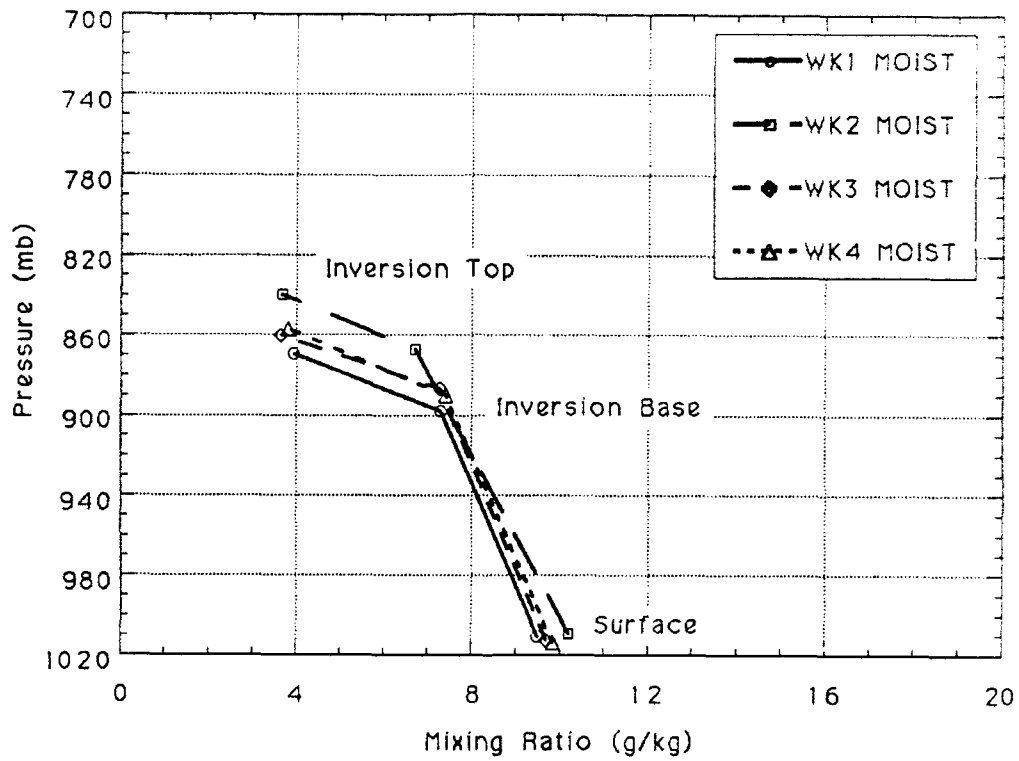


Figure 22: Mean weekly mixing ratio profile of the boundary layer and inversion of subsidence inversions with moist noses. Each week is indicated as follows: Week 1, solid line; Week 2, long dash; Week 3, medium dash; Week 4, short dash.

slightly to 9.8 g/kg in Week 4 (RH = 77%).

The mean weekly subsidence inversion base pressure is 909 mb (1140 m) in Week 1, decreases to 867 mb (1325 m) in Week 2, increases to 887 mb (1315 m) in Week 3, and increases slightly to 890 mb (1230 m) in Week 4. The mean weekly temperature of the subsidence inversion base is 9.5° C in Week 1, decreases to 8.8° C in Week 2, increases to 10.3° C in Week 3, and decreases to 9.5° C in Week 4. The mean weekly mixing ratio at the base of the subsidence inversion is 7.3 g/kg in Week 1, decreases to 6.7 g/kg in Week 2, increases to 7.3 g/kg in Week 3, then increases slightly to 7.4 g/kg in Week 4. The mean weekly relative humidity is 86% in Week 1, then lowers to 80% in Weeks 2 and 3, then increases to 87% in Week 4.

The mean weekly top pressure of subsidence inversions with a moist nose present is 870 mb (1412 m) in Week 1, decreases to 840 mb (1595 m) in Week 2, then increases to 860 mb (1575 m) in Week 3 and 857 mb (1550 m) in Week 4. The mean weekly temperature of the subsidence inversion top is 12.1° C in Week 1, decreases to 11.3° C in Week 2, increases to 13.3° C in Week 3, and decreases again to 12.5° C in Week 4. The mean weekly mixing ratio at the top of the subsidence inversion is 3.9 g/kg in Week 1, decreases slightly to 3.7 g/kg in Week 2 and 3.6 g/kg in Week 3, then increases slightly to 3.8 g/kg in Week 4. The mean weekly relative humidity is 38% in Week 1, decreases to 36% in Week 2, then to 32% in Week 3, and increases to 35% in Week 4.

The mean weekly inversion strength for subsidence inversions with a moist nose present is 0.223 K/mb (0.96° C/100 m) in Week 1, decreases to 0.204 K/mb (0.92° C/100 m) in Week 2, increases to 0.244 K/mb (1.15° C/100 m) in Week 3, and decreases again to

0.225 K/mb (0.94° C/100 m) in Week 4.

Mean profiles of the thermodynamic structure of subsidence inversions with moist noses were examined to provide climatological information about these subsidence inversions. The next section (4.2) will examine the mean thermodynamic structure of subsidence inversions without moist noses. A following section (4.3) will compare these subsidence inversions without moist noses with subsidence inversions with moist noses.

4.2 Climatology of Subsidence Inversions Without Moist Nose Structure

Mean profiles of temperature and mixing ratio at the surface, inversion base and inversion top for subsidence inversions without moist noses present are shown in Figures 23 and 24. The mean thermodynamic structure of these soundings is typically the one used in boundary layer and climate modelling. The mean temperature and mixing ratio at the surface for these soundings are 17.4° C and 9.6 g/kg, respectively (RH = 77%). The mean pressure of the base of the subsidence inversion without a moist nose present is 846 mb (1618 m). The mean temperature and mixing ratio at the base of the subsidence inversion are 6.9° C and 5.7 g/kg, respectively (RH = 76%). The mean pressure of the top of the subsidence inversion is 813 mb (1938 m). The mean temperature and mixing ratio at the top of the subsidence inversion are 10.4° C and 2.7 g/kg, respectively (RH = 27%). The mean inversion strength for subsidence inversions without a moist nose present is 0.276 K/mb (1.09° C/100 m).

In the previous section, diurnal variations of variables at the surface, subsidence inversion

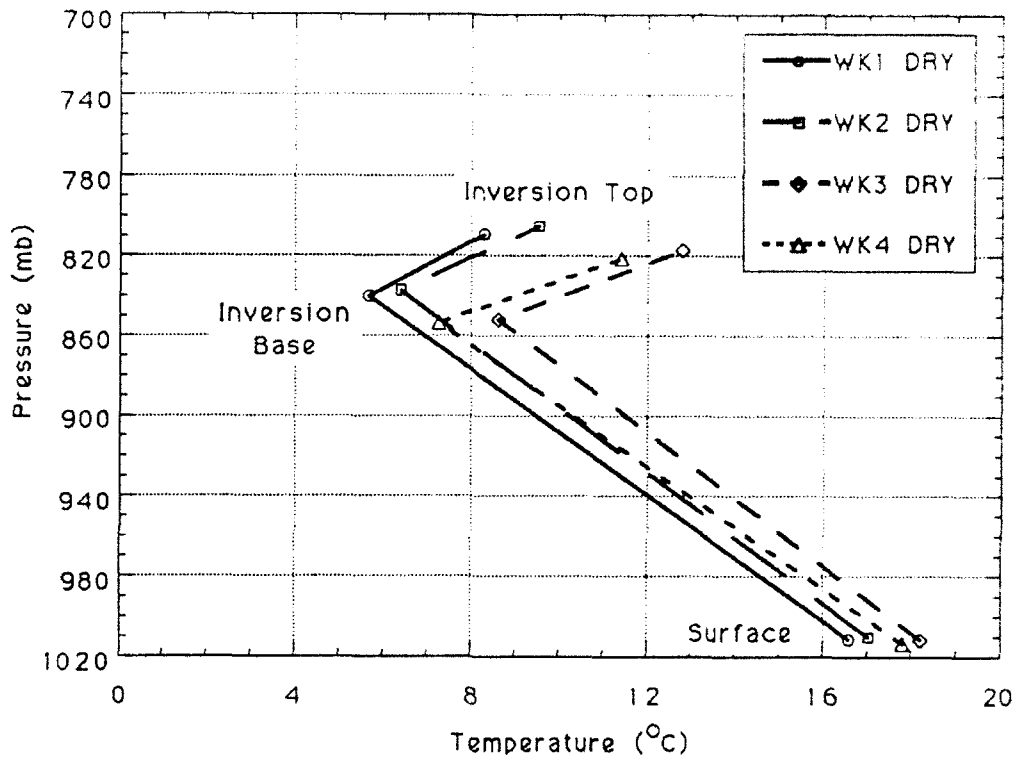


Figure 23: Mean temperature profile of boundary layer and inversion for all subsidence inversions without a moist nose present for all times (solid line), 00 UTC (long dash), 12 UTC (short dash).

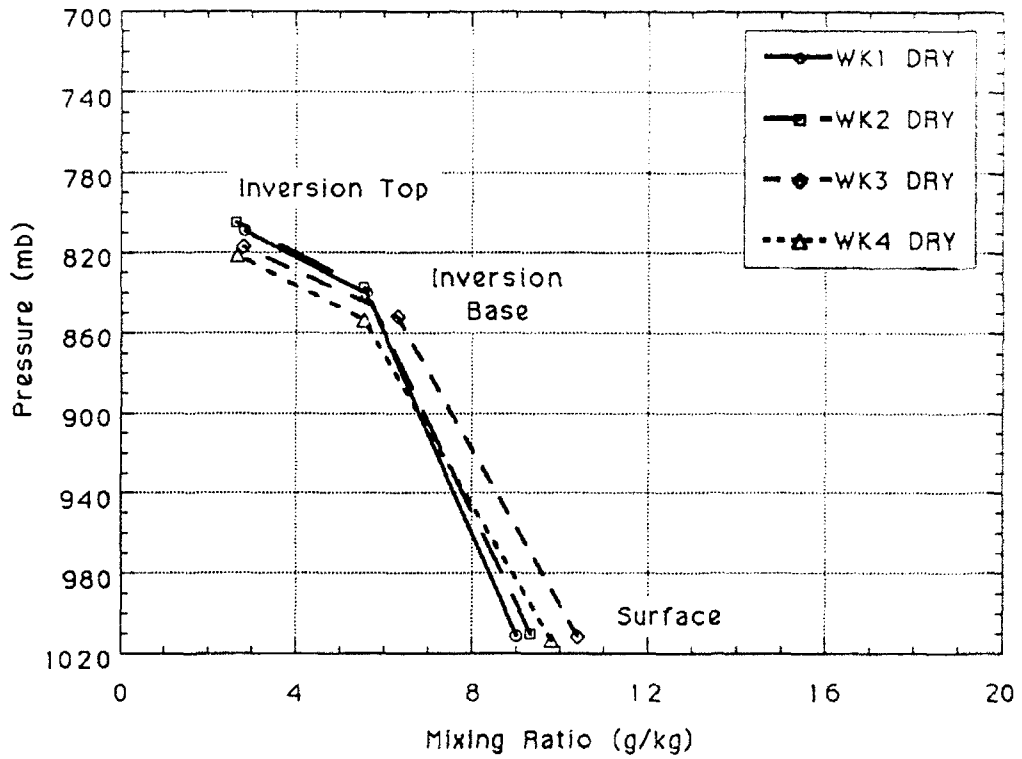


Figure 24: Mean mixing ratio profile of boundary layer and inversion for all subsidence inversions without a moist nose present for all times (solid line), 00 UTC (long dash), 12 UTC (short dash).

base and top were analyzed for all subsidence inversions with moist noses so that they could be compared to subsidence inversions without moist noses. So, the diurnal variations of the same variables for subsidence inversions without moist noses are given here. The mean surface temperature increases from 17.0°C at 00 UTC to 17.7°C at 12 UTC. Again, this mean difference is due to normal daytime heating at the surface. The mean surface mixing ratio decreases from 9.7 g/kg at 00 UTC to 9.0 g/kg at 12 UTC. The mean relative humidity is 80% at 00 UTC and decreases to 74% at 12 UTC. As in the case of the mean subsidence inversion base for soundings with moist noses, between 00 UTC and 12 UTC, the subsidence inversion base pressure of soundings without moist noses decreases from 847 mb (1596 m) to 844 mb (1641 m). Again, with the assumption that increased mixing is occurring in the boundary layer during the day, a 0.7°C increase in surface temperature would result in a 6 mb lowering in the inversion base pressure, which is the same order of magnitude with the findings above.

The mean inversion base temperature and mixing ratio for subsidence inversions without a moist nose present at 00 UTC are 7.1°C and 6.0 g/kg , respectively, and are 6.7°C and 5.4 g/kg , respectively, at 12 UTC. The mean relative humidity at 00 UTC is 78% and decreases to 73% at 12 UTC.

The mean inversion top pressure for subsidence inversions without moist noses decreases from 816 mb (1900 m) at 00 UTC to 811 mb (1976 m) at 12 UTC. The mean inversion top temperature and mixing ratio at 00 UTC are 10.3°C and 3.0 g/kg , respectively (RH = 30%). The mean mixing ratio at the top of the subsidence inversion decreases to 2.4 g/kg at 12 UTC, but the mean temperature at the top of the subsidence inversion increases slightly

to 10.5°C (RH = 24%).

The mean inversion strength for subsidence inversions without moist noses at 00 UTC is 0.280 K/mb ($1.13^{\circ}\text{C}/100\text{ m}$) and decreases to 0.273 K/mb ($1.05^{\circ}\text{C}/100\text{ m}$) by 12 UTC.

Mean weekly temperature and mixing ratio profiles for subsidence inversions without moist noses are shown in Figures 25 and 26. The mean weekly surface temperature increases from 16.6°C in Week 1 to 17.0°C in Week 2, then increases to 18.2°C in Week 3, and decreases to 17.8°C in Week 4. The mean weekly mixing ratio is 9.0 g/kg in Week 1 (RH = 75%), increases to 9.3 g/kg in Week 2 (RH = 77%), then increases again to 10.4 g/kg in Week 3 (RH = 78%), then decreases to 9.8 g/kg in Week 4 (RH = 76%).

The mean weekly subsidence inversion base pressure is 840 mb (1657 m) in Week 1, decreases slightly to 837 mb (1690 m) in Week 2, increases to 852 mb (1540 m) in Week 3, and increases slightly to 853 mb (1579 m) in Week 4. The mean weekly temperature of the subsidence inversion base is 5.7°C in Week 1, increases to 6.4°C in Week 2, then to 8.6°C in Week 3, and lowers to 7.3°C in Week 4. The mean weekly mixing ratio at the base of the subsidence inversion is 5.6 g/kg in Week 1, decreases slightly to 5.5 g/kg in Week 2, increases to 6.3 g/kg in Week 3, and decreases to 5.5 g/kg in Week 4. The mean weekly relative humidity is 80% in Week 1, then lowers to 76% in Week 2, lowers slightly to 75% in Week 3, then to 73% in Week 4.

The mean weekly top pressure of subsidence inversions without a moist nose present is 809 mb (1974 m) in Week 1, decreases slightly to 805 mb (2013 m) in Week 2, increases to 817 mb (1891 m) in Week 3, and increases slightly to 821 mb (1876 m) in Week 4. The mean weekly temperature of the subsidence inversion top is 8.3°C in Week 1, increases to

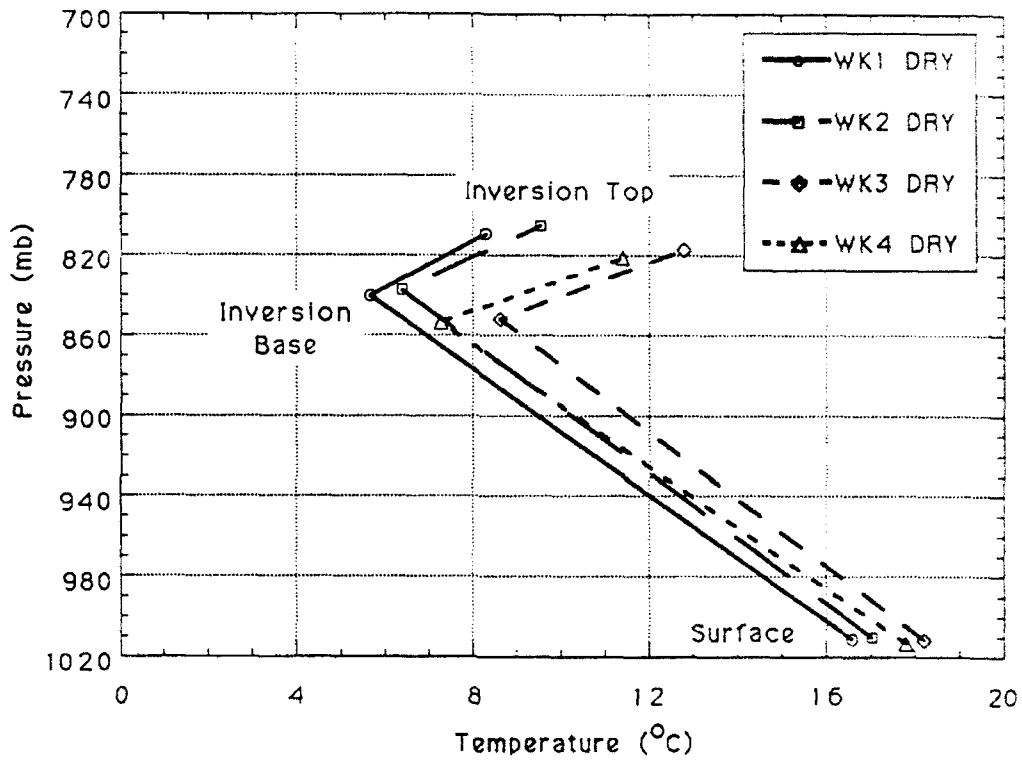


Figure 25: Mean weekly temperature profile of the boundary layer and subsidence inversion of subsidence inversions without moist noses. Each week is indicated as follows: Week 1, solid line; Week 2, long dash; Week 3, medium dash; Week 4, short dash.

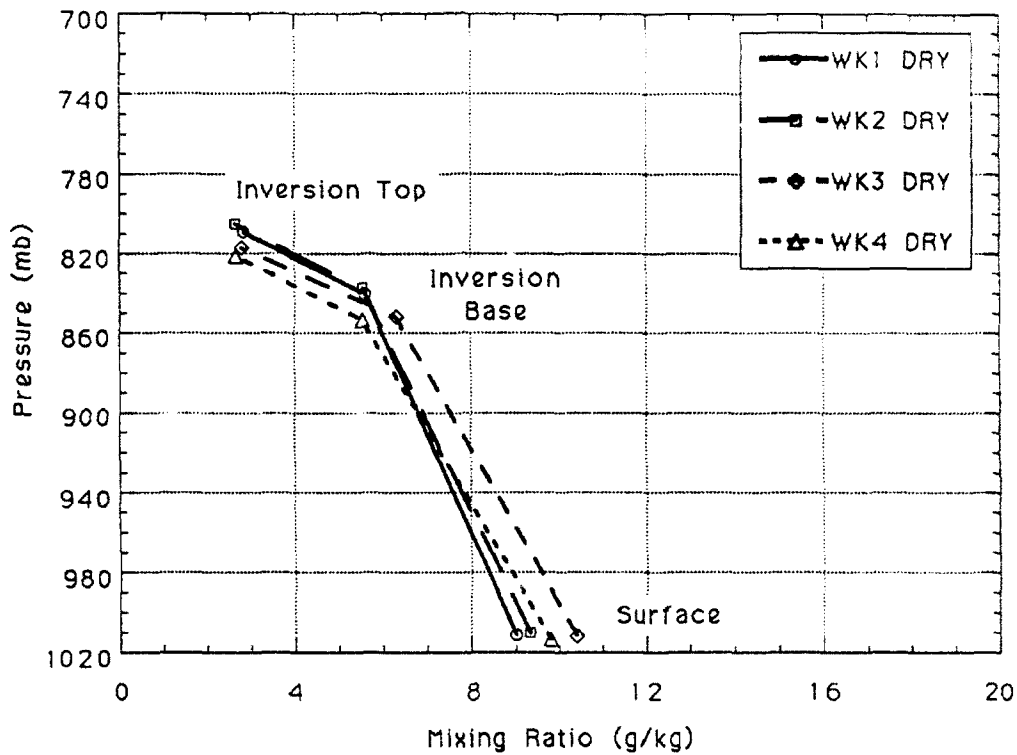


Figure 26: Mean weekly mixing ratio profile of the boundary layer and subsidence inversion of subsidence inversions without moist noses. Each week is indicated as follows: Week 1, solid line; Week 2, long dash; Week 3, medium dash; Week 4, short dash.

9.5° C in Week 2 and to 12.8° C in Week 3, then lowers to 11.4° C in Week 4. The mean weekly mixing ratio at the top of the subsidence inversion is 2.8 g/kg in Week 1, 2.6 g/kg in Week 2, 2.8 g/kg in Week 3, and 2.7 g/kg in Week 4. The mean weekly relative humidity decreases from 32% in Week 1 to 28% in Week 2, to 24% in Week 3, then increases slightly to 25% in Week 4.

The mean weekly inversion strength for subsidence inversions without moist noses increases from 0.232 K/mb (0.82° C/100 m) in Week 1 to 0.270 K/mb (0.96° C/100 m) in Week 2, to 0.297 K/mb (1.20° C/100 m) in Week 3, then to 0.306 K/mb (1.38° C/100 m) in Week 4.

4.3 Differences Between the Thermodynamic Structure of Subsidence Inversions With and Without Moist Noses

In preparation for the discussion of the possible causes of the moist nose structure in Chapter 5, differences in the thermodynamic structure between subsidence inversions with moist noses above are compared to the thermodynamic structure of subsidence inversions without a moist nose above. The most notable difference is that subsidence inversions without moist noses are slightly stronger than those with moist noses by 0.049 K/mb (see Figure 27). Diurnally, subsidence inversions without moist noses are slightly stronger than subsidence inversions with moist noses by 0.050 K/mb at 00 UTC and 0.049 K/mb at 12 UTC. These findings may support the theory that the moisture present above the subsidence inversion may be due to convection through a weak subsidence inversion (Edinger, 1963).

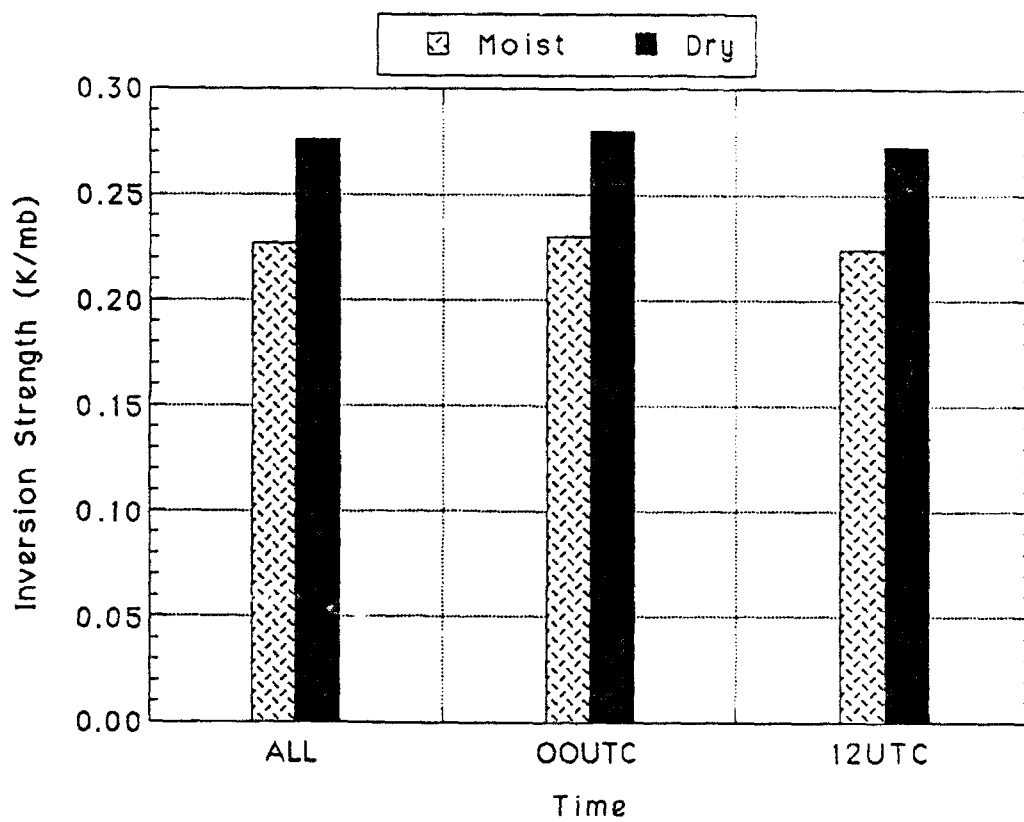


Figure 27: Mean inversion strength of subsidence inversions with the moist nose (light stippled pattern) and without the moist nose present (grey pattern) for all times, 00 UTC and 12 UTC.

Figure 28 shows the mean weekly inversion strength for inversions with and without the moist nose. Again, inversions without the moist nose are slightly stronger than those with the moist nose by 0.009 K/mb in Week 1, 0.066 K/mb in Week 2, 0.053 K/mb in Week 3, and 0.081 K/mb in Week 4.

Another noticeable difference between subsidence inversions with and without moist noses is that the mean base pressure of subsidence inversions with a moist noses is lower than the mean base pressure of inversions without the moist nose. The mean inversion base pressure of the subsidence inversions with the moist nose present is 40 mb lower (363 m higher) than those without the moist nose. Figure 29 shows a comparison of the temperature and mixing ratio of subsidence inversions with a moist nose present to subsidence inversions without the moist nose. Also, at the inversion base, the temperature and mixing ratio for moist nose inversions are 2.7° C and 1.5 g/kg higher, respectively, than inversions without the moist nose present. The pressure at the top of the subsidence inversion is 44 mb lower (400 m higher) for subsidence inversions with moist noses than those without. The mean temperature and mixing ratio at the top of the inversion are 2.1° C and 1.1 g/kg higher, respectively, for subsidence inversions with moist noses than those without. The mean inversion strength is 0.049 K/mb higher for subsidence inversions without moist noses than those with. As mentioned in Chapter 3, the overall mean boundary layer is relatively stable. This is also true for the boundary layers associated with subsidence inversions with and without moist noses. The mean potential temperature profile of soundings with and without moist noses is shown in Figure 30. There is little difference in boundary layer stability between the two profiles shown.

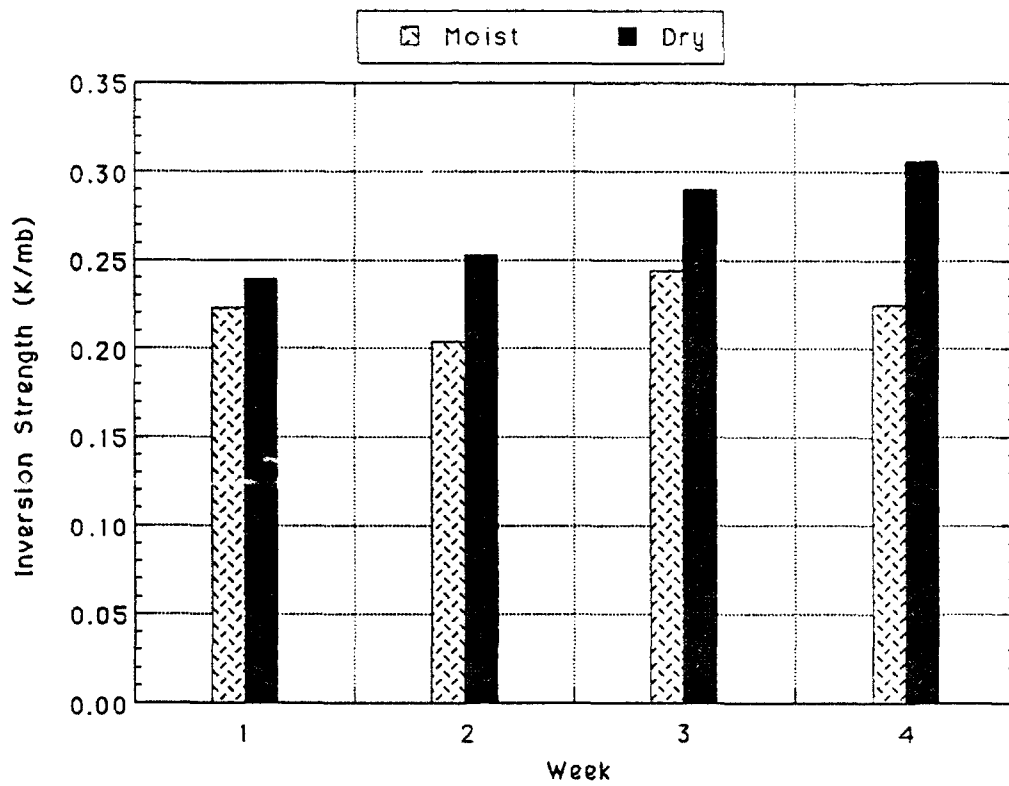


Figure 28: Mean weekly inversion strength of subsidence inversions with (light stippled pattern) and without the moist nose present (grey pattern).

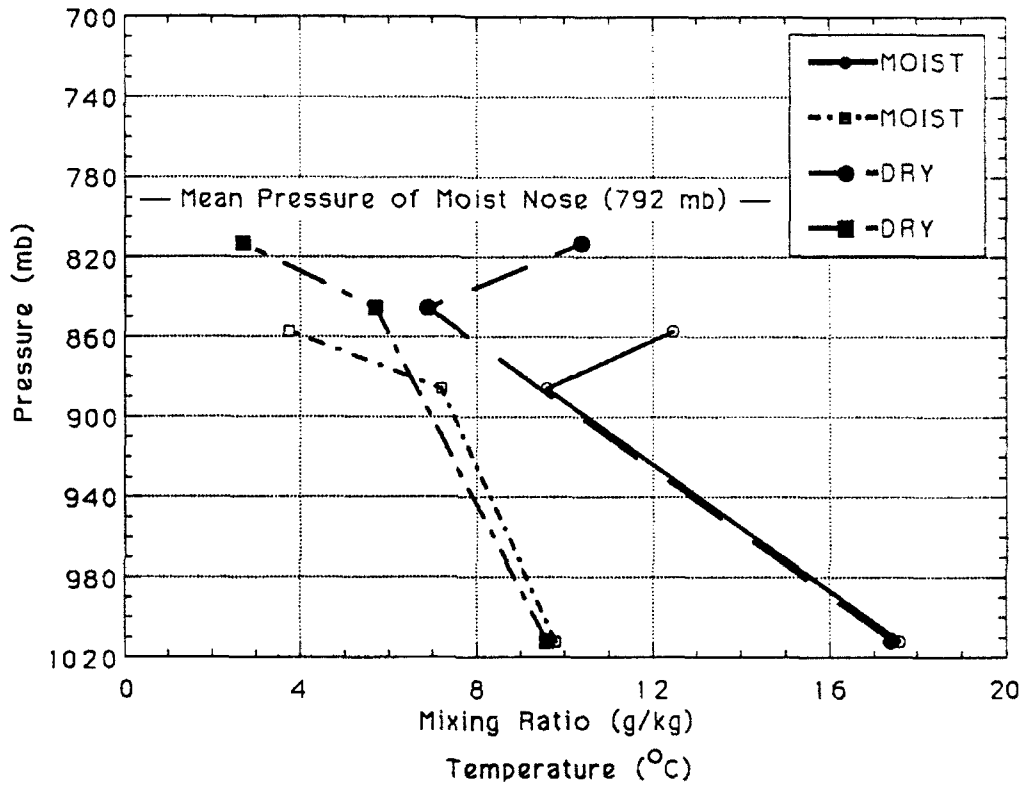


Figure 29: Mean temperature and mixing ratio profiles of boundary layer and inversion for subsidence inversions with the moist nose (solid line and dot-short dash, respectively) and without the moist nose (long dash and dot-long dash, respectively).

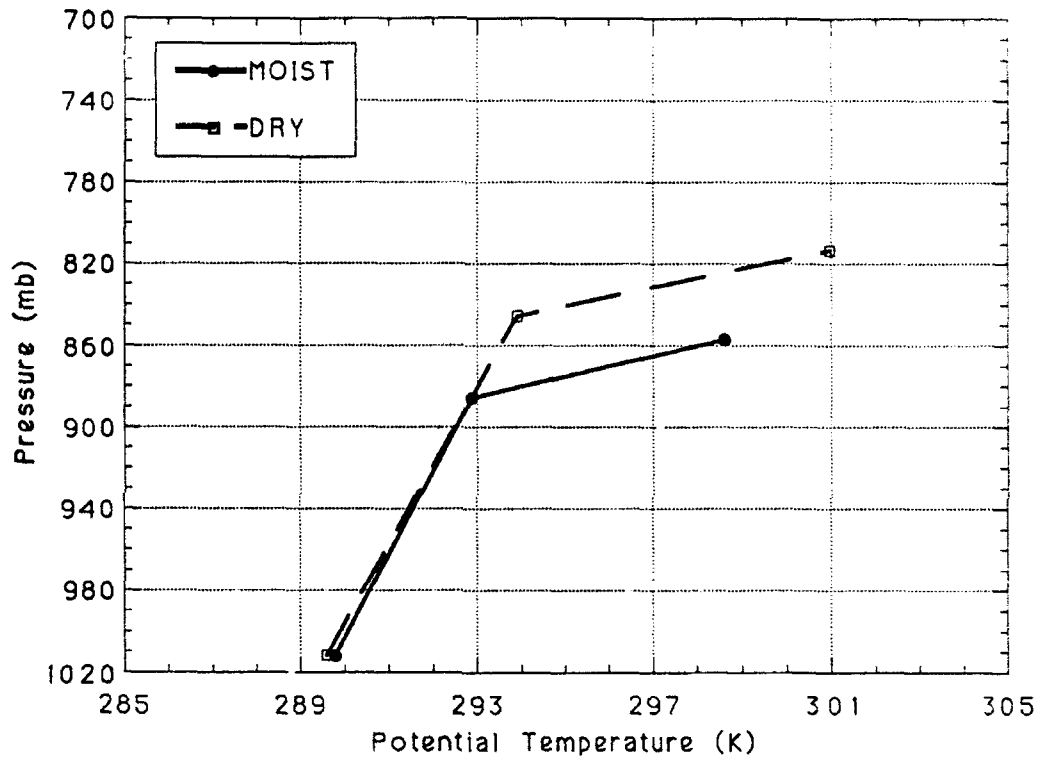


Figure 30: Mean potential temperature profile for subsidence inversions with the moist noses (solid line) and without the moist noses (dashed line).

Differences in diurnal variations of surface temperature and mixing ratio between subsidence inversions with and without moist noses are small. However, diurnal variations of the pressure, temperature, and mixing ratio at the subsidence inversion base and top again indicate differences in the thermodynamic structure between subsidence inversions with and without moist noses. The mean base pressures of subsidence inversions with moist noses at 00 UTC and 12 UTC are lower (higher) by 46 mb (413 m) and 34 mb (296 m), respectively, than those without. The mean temperatures at the base of the subsidence inversions with a moist nose at 00 UTC and 12 UTC are 2.5° C and 1.2° C higher, respectively, than those without moist noses. The mean mixing ratio at the subsidence inversion base is higher than the value at the base of subsidence inversions without moist noses by 1.2 g/kg at 00 UTC ($\Delta RH = 6\%$) and by 2.8 g/kg at 12 UTC ($\Delta RH = 8\%$). (Note: ΔRH is defined as the magnitude of the difference between the value of the relative humidity at a particular level of subsidence inversions with moist noses and subsidence inversions without moist noses.) The mean top pressure of subsidence inversions with moist noses are lower (higher) by 49 mb (434 m) at 00 UTC and 37 mb (354 m) at 12 UTC than subsidence inversions without moist noses. The mean temperature at the base of the subsidence inversions with moist noses increases by 2.4° C at 00 UTC and 2.1° C at 12 UTC by than those without moist noses. The mean mixing ratio at the subsidence inversion top is higher than subsidence inversions without moist noses by 1.0 g/kg at 00 UTC ($\Delta RH = 7\%$) and by 1.1 g/kg at 12 UTC ($\Delta RH = 7\%$).

The mean weekly temperature and mixing ratio profiles for subsidence inversions with and without moist noses are shown in Figures 31 and 32. Week by week, the base of the

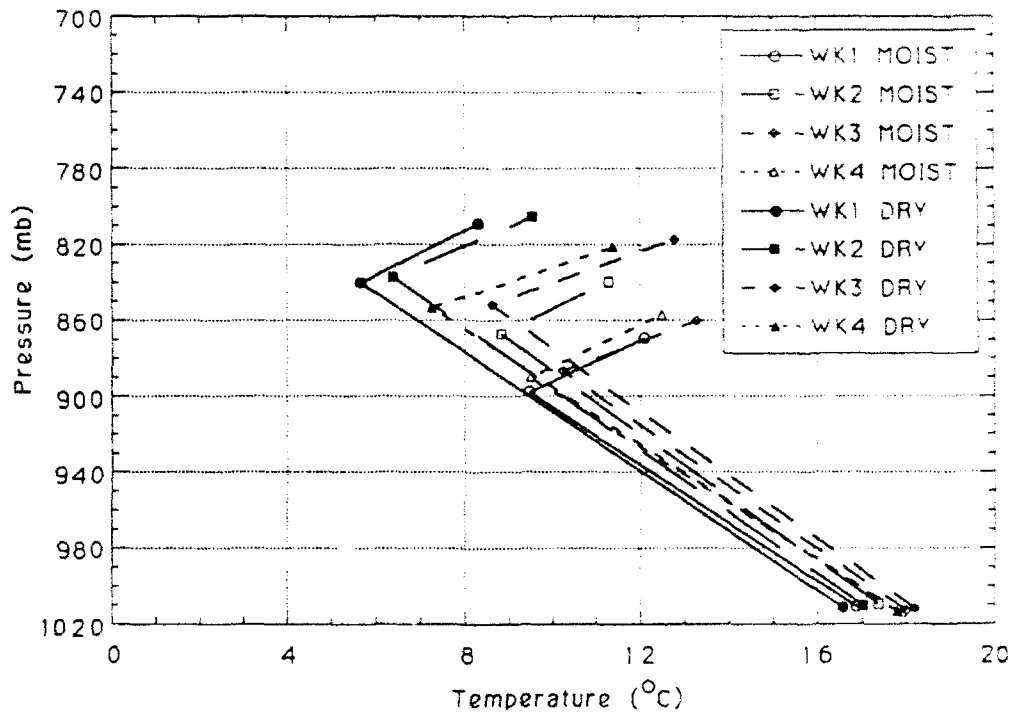


Figure 31: Mean weekly temperature profile for subsidence inversions with the moist nose (plots with hollow symbols) and without the moist nose (plots with filled symbols).

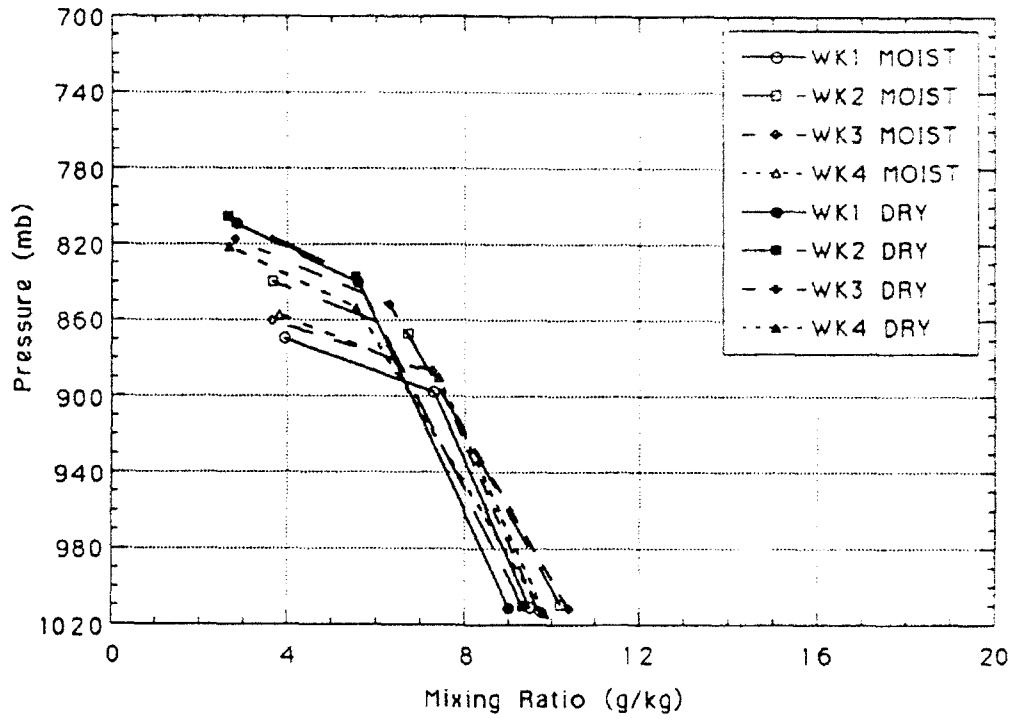


Figure 32: Mean weekly mixing ratio profile for subsidence inversions with the moist nose (plots with hollow symbols) and without the moist nose (plots with filled symbols).

subsidence inversions with moist noses are 30 mb (365 m) to 60 mb (517 m) higher (lower) than subsidence inversions without moist noses. Mean weekly temperatures and mixing ratios of the inversion base of subsidence inversions with moist noses are 1.7° C to 3.8° C warmer and 1.0 g/kg to 1.9 g/kg higher, respectively, than subsidence inversions without moist noses.

The top of the subsidence inversions with moist noses are 35 mb (418 m) to 61 mb (562 m) higher (lower) than subsidence inversions without moist noses. Mean weekly temperatures and mixing ratios of the inversion top of subsidence inversions with moist noses are 0.5° C to 3.8° C higher and 0.8 g/kg to 1.1 g/kg higher, respectively, than subsidence inversions without moist noses. ΔRH varies between 6% and 10%.

From what has been examined, there are some notable differences in pressure, strength and temperature profiles between subsidence inversions with moist noses present and subsidence inversions without moist noses present. Also, climatological information of the moist nose, its mean position and mixing ratio, has been presented to show the complex structure that seems to exist in many cases above the subsidence inversion. Differences in mean inversion strength between subsidence inversions with moist noses and subsidence inversions without moist noses suggest that the moist nose may be formed from convected moisture from the marine boundary layer (confirming Edinger's hypothesis). The relative humidities at the base and top of subsidence inversions are higher for subsidence with moist noses than subsidence inversions without moist noses. Edinger's theory will be examined in detail in the next chapter, as well as other possible sources of the moisture in the moist nose.

Chapter 5

Source of Moisture Above the Subsidence Inversion

As mentioned before in Chapter 4, Edinger (1963) proposed that the origin of the moist nose above the subsidence inversion was from convective transport from the boundary layer through a weakened subsidence inversion. Several methods are employed to examine this theory with the Lajes radiosonde data. Correlations are examined between the amount of moisture at the moist nose and the subsidence inversion strength. If a significant negative correlation exists, then it is possible that the moist nose was created by moisture below the subsidence inversion rising through the subsidence inversion layer via convective transport. To determine if a relationship exists between boundary layer mixing and the presence of the moist nose, potential temperature at the level of the moist nose is correlated with the potential temperature at the surface, and equivalent potential temperature at the moist

nose is correlated with the equivalent potential temperature at the surface. Also, mixing ratio at the level of the moist nose is correlated with the mixing ratio at the surface. Finally, a conserved variable diagram is used to examine the theory that moisture from below the subsidence inversion penetrated through the inversion to produce the moist nose above the inversion.

Figure 33 shows a scatter diagram of the mixing ratio in the moist nose above the subsidence inversion and subsidence inversion strength. A simple linear regression was performed. The correlation coefficient was -0.139 and the least squares regression coefficient was only 0.020. A *t*-test used for the determination of variance revealed no significance to this correlation at the 95% confidence level. Lag correlations were also performed to determine if any correlation exists between the amount of moisture present in the moist nose at a particular time and the inversion strength 12 and 24 hours prior to that time. The results produced correlation coefficients for 12- and 24-hour time lag of -0.049 and -0.092, respectively, with no significance at the 95% confidence level.

Correlations between the potential temperature in the moist nose with the potential temperature at the surface was 0.153. At the 95% confidence level, no significance was found to this correlation. The correlation between the equivalent potential temperature at the surface and the equivalent potential temperature in the moist nose was 0.326. At the 95% confidence level, this weak linear relationship was significant. However, it only explains 11% of the variance. The correlations of the moist nose mixing ratio with the surface mixing ratio was 0.230. Again, at the 95% confidence level, this correlation was significant, but explained only 5% of the variance.

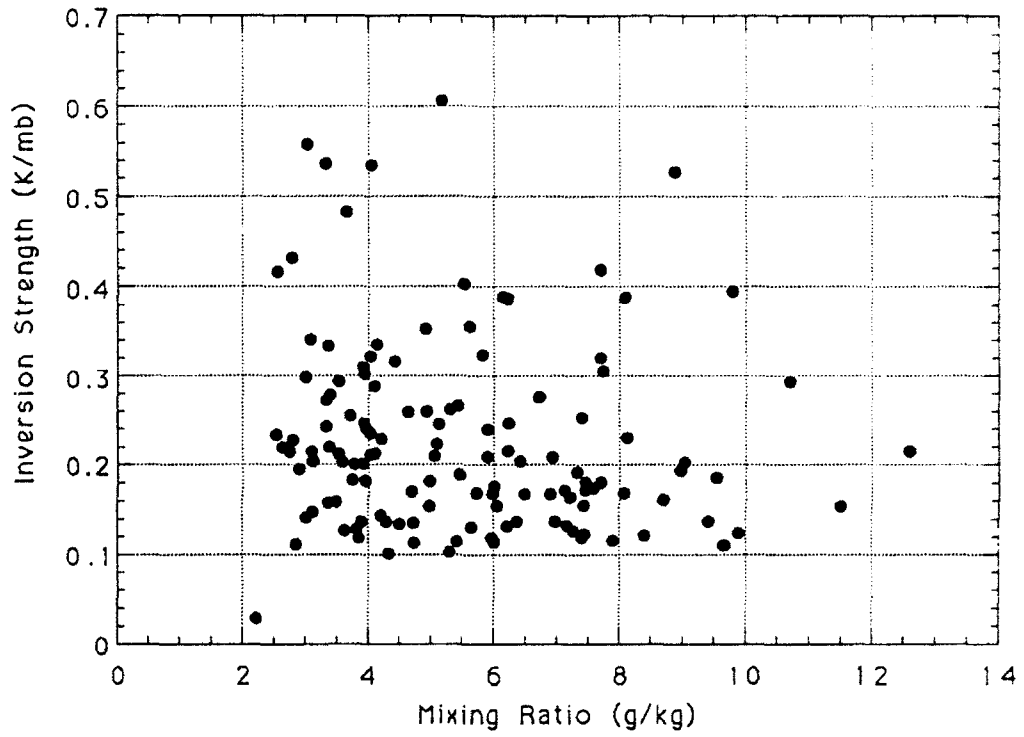


Figure 33: Scatter diagram of mixing ratio (g/kg) above the subsidence inversion and subsidence inversion strength (K/mb).

Correlation coefficients between the mixing ratio in the moist nose and inversion strength indicate that no relationship seems to exist between the two. The correlation between potential temperature in the moist nose and the potential temperature at the surface show similar results. Significance does exist between the correlation of the equivalent potential temperatures at the surface and in the moist nose, and the correlation between the surface and moist nose mixing ratio. However, these weak correlations explain minimal amounts of variance.

To further examine the significance of the correlations presented above and Edinger's theory that the moist nose above the subsidence inversion was created by convective transport of moisture through a weakened inversion, a conserved variable diagram is used. Conserved variable diagrams are useful for studying boundary layer processes (Stull, 1988). Betts (1985) and Betts and Albrecht (1987) made use of conserved variable diagrams, "conserved parameter plots," to study the boundary layer processes. Variables that are conserved during moist and dry adiabatic conditions are used, i.e. equivalent potential temperature and total mixing ratio. For this study, equivalent potential temperature and mixing ratio are used. Mixing ratio is used instead of total mixing ratio because the regime is characteristic of shallow clouds and partly cloudy conditions, so the liquid water content is low. Therefore, total mixing ratio is approximated by mixing ratio. Conserved variable diagrams reduce convective transport in a partially cloudy boundary layer to a simple mixing process. If the plot of equivalent potential temperature and mixing ratio fall on a straight line (called the mixing line) through the boundary layer and subsidence inversion and into the free atmosphere above, the mixing line schematically represents the incorporation of air

from the boundary layer into the free atmosphere above the subsidence inversion (Kloesel, 1987).

Figure 34 shows a conserved variable diagram of mixing ratio and equivalent potential temperature from the Lajes radiosonde data. The mean values of mixing ratio and equivalent potential temperature from 00 UTC, 12 UTC, and Weeks 1 to 4 are plotted for the surface, subsidence inversion base and top, and the level at which a moist nose was present. Assuming that mixing is occurring in the marine boundary layer, the mixing line can be drawn between the surface values and the inversion base values. If mixing incorporates air from the subsidence inversion, then the mixing line can be extended to include the inversion top. In Figure 34, a least squares fit of the surface values, subsidence inversion base and top values gives a regression coefficient of 0.936, indicating a strong linear relationship in the data and a validation of the boundary layer mixing assumption made above. However, if the assumption is made that the convective transport of moisture is strong enough to continue through the subsidence inversion to the typical height of the moist nose seen in the Lajes data, then one would expect that when the mean equivalent potential temperature and mixing ratio of the moist nose are plotted on the conserved variable diagram, the points would lie on the least squares regression line computed above. Figure 34 shows they do not.

Summarizing the results from above, there does not seem to be any correlation between the moisture below or across the subsidence inversion and the moisture in the moist nose above the inversion, whether the moisture and strength of the subsidence inversion were matched at the same time or lagged 12 and 24 hours. Therefore, the possibility that the

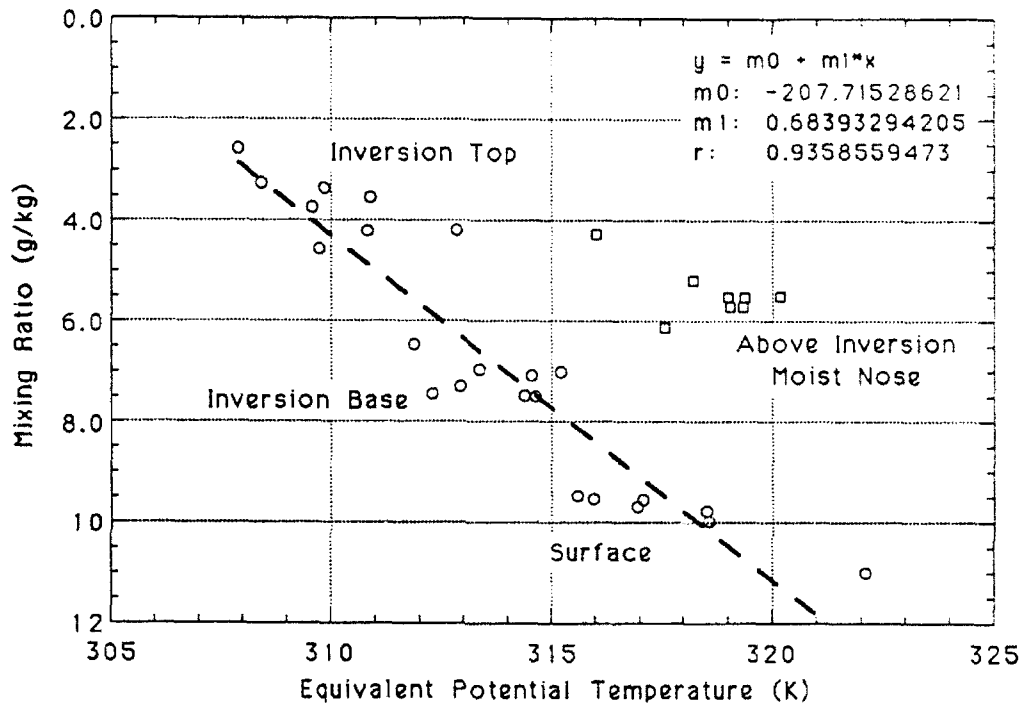


Figure 34: Conserved variable diagram of the mean values of mixing ratio and equivalent potential temperature at the surface, inversion base and top and in the moist nose for all times, 00 UTC, 12 UTC, and Weeks 1 through 4 for all subsidence inversions with moist noses. The dashed line is a least-squares fit of the surface, inversion base and top values.

moist nose was created by convective transport through a weakened inversion seems unlikely. A significant correlation does not exist between the potential temperature in the moist nose and the potential temperature at the surface or the change of potential temperature across the inversion. The conserved variable diagram further disproves Edinger's theory by showing that the moist nose does not contain the properties of the air mixed from below.

One possible explanation for the existence of the moist nose could be residual moisture from the deeper boundary layers observed when no moist noses was present (Chapter 4). However, this scenario is not likely since the mean height of the moist nose is 21 mb lower (270 m higher) than the subsidence inversion top in non-moist nose cases.

Another possible source for the moisture above the subsidence inversion was investigated by Kloesel (1992) during FIRE. Off the California coast, large amounts of moisture were detected above subsidence inversions along the eastern periphery along the Pacific Subtropical Anticyclone (PSTA). With the use of satellite data and isentropic trajectory analysis, he found that the moisture appeared to originate in cyclonic disturbances occurring on the western side of the PSTA. Moisture associated with these systems then advected around the northern and eastern periphery of the anticyclone, subsiding into the region off the coast of California.

There is a possibility that the moist nose structure found above the subsidence inversions in the eastern Atlantic was created in a similar manner. However, the Atlantic Ocean is smaller in size than the Pacific Ocean, so the moisture source may not be as clearly defined. Figure 35 shows the mean surface pressure pattern for July in the Atlantic and Pacific Oceans. The anticyclone in the Atlantic is weaker than in the Pacific. The PSTA is

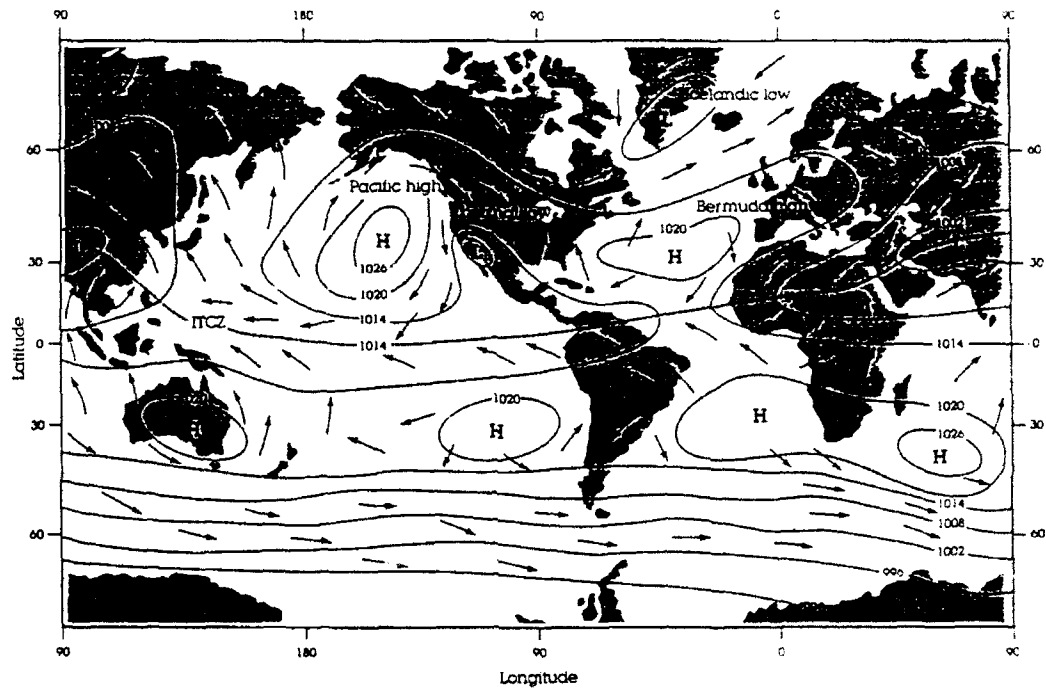


Figure 35: Mean global surface pressure pattern for the month of July (from Ahrens, 1991).

broader, longitudinally and latitudinally, than the Atlantic subtropical anticyclone. Also, the possibility exists that the moisture structure in some of these soundings was caused by water vapor remnants of mid-level cloudiness associated with frontal systems, which advected into the weak or transient subtropical anticyclone. As mentioned in Chapter 3, the transient nature of the subtropical anticyclone was observed on several occasions in the data. Any strong frontal activity moving through the Atlantic appears to weaken and displace the subtropical anticyclone, confirmed by the observance of soundings with frontal inversions noted in Chapter 3. This same frontal activity does not appear to be as prevalent in the Pacific. In this data, however, no apparent relationship between the daily surface pressure patterns and the presence of the moist nose was observed.

Chapter 6

Conclusion

Since data is not readily available over the entire Atlantic Ocean, little is known about the characteristics of the Atlantic Subtropical Anticyclone. Experiments such as GATE, BOMEX, and ATEX have provided useful data to study the trade cumulus regime and the trade wind inversion associated with the anticyclone in the subtropical regions of the Atlantic, but information regarding the subsidence inversion regime along the eastern periphery of the Atlantic Subtropical Anticyclone is scarce. FIRE, conducted in the Pacific Ocean, has provided useful information about the subsidence inversion regime in the eastern North Pacific.

In addition, it was observed in FIRE that the subsidence inversion may not display the "classic" temperature and moisture profiles found in Figure 2 of Chapter 1. The moisture profile may be more complex. Stull (1988) states that water vapor is the most important constituent controlling the infrared radiation budget in the boundary layer. In light of the data about the moist nose presented in this study, cloud and radiative parameterizations in

climate models would need to be improved to resolve the observed atmospheric conditions. Hopefully, the ASTEX data will provide useful information about the moisture profile above subsidence inversions for such parameterizations.

This study is the first evaluation of the climatology of the subsidence inversion structure in the eastern Atlantic. Data from Lajes Air Base, located along the eastern periphery of the subtropical anticyclone, was used to provide information about the subsidence inversion, its climatology and characteristics, and to show the existence of the moist layer observed above the subsidence inversion.

From the soundings available at Lajes for an 11-year period, it was seen that the dominant inversion was the subsidence inversion, although other inversions were found. Diurnal variations of temperature and mixing ratio at the surface, subsidence inversion base and top, behaved in a explainable manner. The mean weekly values of temperature and mixing ratio at the subsidence inversion base and top were not as easy to explain. This may be due to the transient nature of the subtropical anticyclone in the Atlantic. The mean strength of the subsidence inversion increased through the month, indicating the influence and establishment of the subtropical anticyclone.

It was discovered from the Lajes data that there was a complex moisture structure above the subsidence inversion similar to the one found in the Pacific. Differences were discussed between subsidence inversions with and without moist noses. Subsidence inversions with moist noses were generally lower, weaker and more moist than subsidence inversions without moist noses.

One possible explanation for the source of moisture above the subsidence inversion was

given by Edinger (1963). From his explanation, the moisture could have come from below a weaker subsidence inversion via convective transport. The strongest evidence used to disprove Edinger's theory was the conserved variable diagram presented in Chapter 5, which indicated that the existence of the moist nose was not due to upward mixing of moisture from the marine boundary layer. In addition, low correlations of surface mixing ratio and inversion strength to the amount of moisture present at the moist nose concluded that there was no relationship between them. Also, the correlations between surface potential temperature and the potential temperature at the moist nose, and surface equivalent potential temperature and the equivalent potential temperature at the moist nose both had low correlations.

Another possible explanation for the source of moisture above the subsidence inversion was given by Kloesel (1992). He examined the possibility that the origin of the moist nose in the eastern Pacific was from the western side of the PSTA. The data set used for this study was not extensive enough to examine if a similar scenario occurs in the Atlantic. When the data from ASTEX becomes available, further research should be accomplished to: 1) verify the existence of the moist nose structure above the subsidence inversion in the Atlantic, 2) determine the origin of the moisture above the subsidence inversion, 3) determine the horizontal extent of the moist layer, which, if large enough, could affect boundary layer model parameters, and 4) determine how the presence of the moist nose alters the radiation budget and what differences, radiatively, there are between the cloudless moist nose and a cloud-topped boundary layer. With this information and information about the possible interaction between the moist layer and cloud-topped marine boundary layer,

cloud and radiative parameters in boundary layer models could be updated, improving the output. Since climate models have lower temporal and spatial resolution than boundary layer models, the presence of the moist nose may not impact climate models directly. the moist nose feature is too small, spatially, to be resolved in current climate models. However, if the presence of the moist nose affects the cloudiness in the boundary layer, then the output from the boundary layer models could provide better parameterization schemes of the cloud-topped marine boundary layer for climate models, thus improving climate model output.

References

- Ahrens, C. D., 1991: *Meteorology Today: An Introduction to Weather, Climate, and the Environment*. West Publishing Company, St. Paul, MN.
- Augstein, E., H. Riehl, F. Ostapoff, and V. Wagner, 1973: Mass and energy transports in an undisturbed Atlantic trade-wind flow. *Mon. Wea. Rev.*, **101**, 101-111.
- , H. Schmidt, and F. Ostapoff, 1974: The vertical structure of the atmospheric planetary boundary layer in undisturbed trade winds over the Atlantic Ocean. *Bound.-Layer Meteor.*, **6**, 129-150.
- Betts, A. K., 1985: Mixing line analysis of clouds and cloudy boundary layers. *Journ. Atmos. Sci.*, **42**, 2751-2763.
- , and B. A. Albrecht, 1987: Conserved parameter analysis of the convective boundary layer thermodynamic structure over the tropical oceans. *Journ. Atmos. Sci.*, **44**, 83-99.
- desJardins, M. L., K. F. Brill, and S. S. Schotz, 1991: *NASA Technical Memorandum 4260 - GEMPAK5 User's Guide, Version 5.0*. National Aeronautics and Space Administration, Greenbelt, Maryland.
- Edinger, J. G., 1963: Modification of the marine layer over coastal southern California. *J. Appl. Meteor.*, **2**, 706-712.
- FIRE Project Office and ASTEX Working Group, 1992: ASTEX Operations Plan.
- House, R. A., Jr. and A. K. Betts, 1981: Convection in GATE. *Rev. of Geophys. and Space Phys.*, **19**, 541-576.
- HQ, Air Weather Service, 1961: Use of the Skew-T, Log-P diagram in analysis and forecasting, vol I, radiosonde analysis. Scott AFB, IL, 6-5 - 6-6.
- Kloesel, K. A., 1987: Analysis of the structure of the convective boundary layer over the tropical Pacific Ocean during 1979. M.S. Thesis, The Pennsylvania State University.

- , and B. A. Albrecht, 1989: Low-level inversions over the tropical Pacific – Thermodynamic structure of the boundary layer and the above-inversion moisture structure. *Mon. Wea. Rev.*, **117**, 87-101.
- , 1992: Above inversion profiles of moisture and ozone observed during FIRE. In press, *Mon. Wea. Rev.*
- Lilly, D. K., 1968: Models of cloud-topped mixed layers under strong inversions. *Quart. J. Roy. Meteor. Soc.*, **94**, 292-309.
- Nitta, T., and S. Esbensen, 1974: Heat and moisture budgets using BOMEX data. *Mon. Wea. Rev.*, **102**, 17-28.
- Randall, D. A., J. A. Coakley, Jr., C. W. Fairall, R. A. Kropfli, and D. H. Lenschow, 1984: Outlook for research on subtropical marine stratiform clouds. *Bull. Amer. Met. Soc.*, **65**, 1290-1301.
- Schwiesow, R. L., S. D. Mayer, V. M. Glover, and D. H. Lenschow, 1990: Intersection of a sloping aerosol layer observed by airborne lidar with a cloud-topped marine boundary layer. *J. Appl. Met.*, **29**, 1111-1119.
- Sommeria, G., J. Slingo, and M. Tiedtke, 1985: Parameterization of the cloud-topped boundary layer in a global forecast model. A workshop on modelling of the cloud-topped boundary layer, Colorado State University, Fort Collins, Colorado.
- Stull, R. B., 1988: *An Introduction to Boundary Layer Meteorology*. Kluwer Academic Publishers, Dordrecht, The Netherlands.

Vita

Captain Mark B. Miller was born in Harrisburg, PA on August 17, 1964. He graduated from Central Dauphin High School, Harrisburg, PA in 1982, and graduated from The Pennsylvania State University in 1986 with a Bachelor of Science degree in Meteorology. Upon graduation, he was commissioned in the United States Air Force as a second lieutenant and was stationed at Langley Air Force Base, Virginia. For a year and 9 months, he was the Wing Weather Officer at the weather station, briefing F-15 pilots for missions and exercises. He then was moved to Headquarters, Tactical Air Command (TAC) at Langley, where he was a forecaster and command briefer to the 4-star general in charge of TAC.